Time and Frequency Domain Analysis of Spike Train and Time Series Data

David M. Halliday and Jay R. Rosenberg

Introduction

The concept of a spike triggered average will be familiar to many neurophysiologists. The first application in neurophysiology by Mendell and Henneman (1968, 1971) was used to examine the magnitude of monosynaptic excitatory postsynaptic potentials (EPSP) from muscle spindle Ia afferents onto homonymous motoneurons, which provided a major piece of evidence in the development of the size principle for motoneuron recruitment (see Henneman and Mendell, 1981). The technique has gained widespread acceptance, and been widely used to investigate the strength of synaptic connections in the mammalian central nervous system (e.g. Watt et al., 1976; Stauffer et al., 1976; Kirkwood and Sears, 1980; Cope et al., 1987), leading to new insights and an increased understanding of basic neurophysiological mechanisms.

The basic principle in the above studies is that averaging of an intracellular recording from a motoneuron triggered by action potentials from a single intact afferent will reveal a waveform which is taken as an estimate of the postsynaptic potential (PSP) for that input. Averaging is required due to the presence of unrelated activity within the cell, which can be regarded as a noise component. Spike triggered averaging can detect weak effects (Cope et al., 1987), averages involving 10^5 or more triggers are commonly used.

A similar procedure is often used to assess the coupling between two simultaneously recorded sequences of action potentials. In this case it is the timing of spikes in one spike train which is averaged with respect to the timing of spikes in a second spike train. This leads to a histogram based measure, frequently referred to as the cross-correlation histogram, which shows the relative timing of spikes in one spike train with respect to a second spike train. First used by Griffith and Horn (1963) to study functional coupling between cells in cat visual cortex, this method has subsequently been widely accepted and used in other areas of neurophysiology (e.g. Sears and Stagg, 1976; Kirkwood and Sears, 1978; Datta and Stephens, 1990).

Spike triggered averaging and cross-correlation histogram analysis can be considered as the detection of a *correlation* between two signals. Both are affected by the presence of noise, particularly when studying weak interactions. In most cases the signals which are being studied contain noise, and can therefore be considered as stochastic processes. The study of stochastic signals, and the detection of correlated activity in the presence of noise are major research areas in engineering and statistics, an extensive literature exists on the related questions of characterizing stochastic signals, and the estimation of correlated activity in the presence of noise (e.g. Brillinger and Tukey, 1984). In this chapter we are concerned with the question: Given two stochastic signals (which

Correspondence to: David M. Halliday, University of Glasgow, Division of Neuroscience and Biomedical Systems, Institute of Biomedical and Life Sciences, West Medical Building, Glasgow, G12 8QQ, UK (phone: +44-141-330-4759; fax: +44-141-330-4100; e-mail: gpaa34@udcf.gla.ac.uk)

can be either a sequence of spike times, or a sampled waveform) then how can these signals, and any correlation between them, be characterized? The *mean* and *variance* of a regularly sampled waveform are useful measures which characterize the distribution of amplitude values. *Auto-spectra* provide a more informative picture of the data, auto-spectral estimates can be interpreted as statistical parameters related to the variance of the signal at discrete frequencies. Similar comments apply to spike train data, which can be treated as a sequence of *point events*, and the distribution of intervals between successive spikes subjected to a similar analysis. The question of correlation between two signals can be considered as an investigation of the joint distribution of two stochastic processes, which leads to covariance analysis and cross-spectral analysis. These concepts will be expanded upon in the following sections, the object of these introductory remarks is to place the problem of assessing the correlation between neurophysiological signals in the domain of engineering and statistics, which allows the extensive methods which have been developed in these fields to be applied to the problem.

An important aspect of studying correlation in the presence of noise is the ability to place some error bounds on parameter estimates. This is often missing in the application of spike triggered averaging and cross-correlation techniques. The use of statistics should form an essential part of any analysis, both for dealing with error and uncertainty, and for testing hypotheses about the correlation structure between signals.

The object of this chapter is to present a framework within which the correlation between spike train data and/or sampled waveform data can be studied, where both time domain and frequency domain measures are used in a complementary fashion to maximise the insight into and inferences from experimental data. In this framework, the spike triggered average and cross-correlation histogram are closely related to cumulant density functions, a time domain parameter estimated from an inverse Fourier transform of a cross-spectrum. A key feature of the framework is the unified aspect for dealing with both spike train, sampled waveform and mixed spike train/waveform data. This is achieved using a Fourier based set of estimation procedures. In this context, a key result is that the large sample statistical properties of the finite Fourier transform of a stochastic signal are simpler than those of the process itself (Brillinger, 1974; 1983) and are the same for both types of data (Brillinger, 1972).

We consider first the analysis of spike train data. Part 1 defines time domain parameters which can be used to assess the correlation between spike trains, describes estimation procedures, based on the cross-correlation histogram, and Example 1 illustrates a sample analysis of two motor unit spike trains. The majority of the chapter is then concerned with a Fourier based framework for dealing with both spike train and waveform data. Part 2 discusses the Fourier transform of both data types, and defines and gives procedures for estimating second order spectra. Part 3 defines parameters which can be used to characterize the correlation between pairs of signals, application of these to different data sets is illustrated in Examples 7–10. Part 4 discusses how to extend the framework to deal with the interactions between several simultaneously recorded signals. Part 5 describes an approach for summarizing the correlation structure between several independent pairs of signals. Part 6 outlines an alternative approach to the analysis of spike train data, based on maximum likelihood methods. In the Concluding Remarks we discuss the limitations of the techniques presented.

In this chapter, the statistical presentation is kept to a minimum, with only the basic definitions and estimation procedures presented. The techniques, however, are presented in sufficient detail to allow the interested reader to undertake the analyses themselves. This chapter summarizes several years of interdisciplinary work, further details can be found in the references cited below, and in the following publications and references cited therein (Rosenberg et al., 1982, 1989, 1998; Halliday et al., 1992, 1995a; Amjad et al., 1997).

PART 1: Time Domain Analysis of Neuronal Spike Train Data

Stochastic Point Process Parameters for Time Domain Analysis of Neuronal Spike Train Data - Definitions

In this section we define a number of time domain parameters, estimates of which can be used to characterize interactions between spike trains. Estimation procedures and the setting of *confidence limits* are described in the next section.

In dealing with neuronal spike train data, the quantities normally available for analysis are the times of occurrence of each spike. The duration of action potentials is short compared with the spacing between, thus the sequences of spike times are normally considered as a series of point events. In addition, the interval between events is not deterministic but contains random fluctuations. We can therefore consider neuronal spike trains (or any other sequence of events which meet these requirements) as realizations of stochastic point processes. A *stochastic point process* may be defined formally as a random non-negative integer-valued measure (Brillinger 1978). In practice this represents the ordered times of occurrence of spikes (or events) in terms of a multiple of the sampling interval, *dt*, which should be chosen sufficiently small such that at most one event occurs in any interval. A point process which satisfies this condition is known as *orderly*.

We further assume that the point process data is *weakly stationary*, i.e. parameters which characterize the data do not change with time, and that widely spaced differential increments are effectively independent. This latter is known as a *mixing condition*. Discussion of these assumptions can be found in Cox and Isham (1980), Cox and Lewis (1972) and Daley and Vere-Jones (1988), and in relation to neuronal spike trains in Conway et al. (1993). The assumption of orderliness is important, since it allows certain point process parameters to be interpreted in terms of expected values or as probabilities (Cox and Lewis, 1972; Srinivasan, 1974; Brillinger, 1975), which provides a useful guide to the interpretation of these parameters.

For a point process, denoted by N_1, the *counting variate* $N_1(t)$ counts the number of events in the interval $(0,t]$. An important elementary function of point processes is the differential increment. The *differential increment* for process N_1 is denoted by $\mathrm{d}N_1(t)$, and defined as $\mathrm{d}N_1(t) = N_1(t, t + dt]$. It can be considered as a counting variate, which counts the number of events in a small interval of duration *dt* starting at time *t*. For an orderly point process, $\mathrm{d}N_1(t)$ will take on the value 0 or 1 depending on the occurrence of a spike in the sampling interval *dt*.

Two simultaneously recorded spike trains can be considered as a realization of a bivariate point process. Let (N_0, N_1) be such a realization of a stationary bivariate point process with differential increments at time *t* given by $\{\mathrm{d}N_0(t), \mathrm{d}N_1(t)\} = \{N_0(t+dt], N_1(t+dt]\}$. Stationarity of (N_0, N_1) implies that the distribution of the differential increments in the intervals $(t, t+dt]$ and $(t+\tau, t+\tau+dt]$ is independent of τ. The following point process parameters may be defined in terms of the differential increments (Brillinger 1975, 1976; Rosenberg et al., 1982, 1989, Conway et al., 1993).

The *mean intensity*, P_1, of the point process N_1 is defined as

$$E\{\mathrm{d}N_1(t)\} = P_1\, dt \tag{1}$$

where E{ } denotes the averaging operator or mathematical expectation of a random variable. The assumption of orderliness allows expression (1) to be interpreted in a probabilistic manner as

$$\mathrm{Prob}\{N_1 \text{ event in } (t, t+dt]\} \tag{2}$$

The mean intensity, P_0, of the point process N_0 is defined in a similar manner. The second order cross-product density at lag u, $P_{10}(u)$, between the two point processes N_0 and N_1 is defined as

$$E\{dN_1(t+u)\,dN_0(t)\} = P_{10}(u)\,du\,dt \tag{3}$$

This expression can be interpreted as

$$\text{Prob}\{N_1 \text{ event in } (t+u, t+u+du] \quad \& \quad N_0 \text{ event in } (t, t+dt]\} \tag{4}$$

The second order product-density functions, $P_{00}(u)$ and $P_{11}(u)$, are defined as in (3) by equating N_0 and N_1. A *conditional mean intensity* can be defined as

$$m_{10}(u) = P_{10}(u)/P_0 \tag{5}$$

which can be interpreted as a conditional probability as

$$\text{Prob}\{N_1 \text{ event in } (t+u, t+u+du] \text{ given an } N_0 \text{ event at } t\} \tag{6}$$

From the mixing condition, the differential increments $dN_1(t+u)$ and $dN_0(t)$ become independent as u becomes large. Therefore we can write

$$\lim_{|u|\to\infty} P_{10}(u) = P_1 P_0 \tag{7}$$

This leads to the definition of the second order *cross-covariance function*, also called the second order *cumulant density function*, $q_{10}(u)$, as

$$q_{10}(u) = P_{10}(u) - P_1 P_0 \tag{8}$$

The two *auto-covariance functions*, $q_{00}(u)$ and $q_{11}(u)$, are defined similarly. This function will tend to zero as $|u| \to \infty$, and has the interpretation

$$\text{cov}\{dN_1(t+u), dN_0(t)\} = q_{10}(u)\,du\,dt \tag{9}$$

where cov{ } denotes covariance. In the case of the individual processes we must write

$$\begin{aligned} \text{cov}\{dN_0(t+u), dN_0(t)\} &= (\delta(u) + q_{00}(u))\,du\,dt \\ \text{cov}\{dN_1(t+u), dN_1(t)\} &= (\delta(u) + q_{11}(u))\,du\,dt \end{aligned} \tag{10}$$

where $\delta(\bullet)$ is a *Dirac delta function* which has to be included to take into account the behavior of the covariance density at u=0.

Estimation Procedures and Confidence Limits for Time Domain Point Process Parameters

The mean intensity, P_1, for a sample of duration R of the point process N_1 can be estimated as

$$\hat{P}_1 = \frac{N_1(\text{R})}{\text{R}} \tag{11}$$

For example, if N_1 is a sample spike train of 60 seconds duration with a sampling interval of 1 millisecond, containing 500 events, then R=60,000 and $\hat{P}_1$ = 500/60000. To distinguish between a parameter and its estimate, we use the notation $\hat{P}_1$ to denote an estimate of the parameter P_1.

Estimates of the second order product densities defined above can be constructed by the following procedure. If we denote the set of spike times for N_0 as $\{r_i\,;\, i=1,\ldots N_0(\text{R})\}$

and the set of spike times for N_1 as $\{s_j\,;\, j=1,\ldots\ N_1(\mathrm{R})\}$, we can construct a counting variate $\mathrm{J}_{10}^{\mathrm{R}}(u)$ such that (Griffith and Horn, 1963; Cox 1965)

$$\mathrm{J}_{10}^{\mathrm{R}}(u) = \#\left\{\left(r_i, s_j\right) \text{ such that } \left(u-\frac{b}{2}\right) < \left(s_j - r_i\right) < \left(u+\frac{b}{2}\right)\right\} \tag{12}$$

where $\#\{A\}$ indicates the number of events in set A. The variate $\mathrm{J}_{10}^{\mathrm{R}}(u)$ counts the number of occurrences of N_1 events falling in a bin of width b, whose midpoint is u time units away from an N_0 event. In the neurophysiological literature, the variate $\mathrm{J}_{10}^{\mathrm{R}}(u)$ is often called the *cross-correlation histogram*. The expected value of this variate is (Cox 1965; Cox and Lewis, 1972)

$$E\left\{\mathrm{J}_{10}^{\mathrm{R}}(u)\right\} \approx b\,\mathrm{R}\,P_{10}(u) \tag{13}$$

This equation illustrates the relationship between the cross-correlation histogram and the second order product density, and leads to the following approximately unbiased estimates for $P_{10}(u)$ and $m_{10}(u)$

$$\hat{P}_{10}(u) = \mathrm{J}_{10}^{\mathrm{R}}(u)/b\mathrm{R} \tag{14}$$

$$\hat{m}_{10}(u) = \mathrm{J}_{10}^{\mathrm{R}}(u)/b N_0(\mathrm{R}) \tag{15}$$

where $\hat{m}_{10}(u)$ denotes an estimate of $m_{10}(u)$. The cumulant density, $q_{10}(u)$, can be estimated using equation (8) as

$$\hat{q}_{10}(u) = \hat{P}_{10}(u) - \hat{P}_1\,\hat{P}_0 = \mathrm{J}_{10}^{\mathrm{R}}(u)/b\mathrm{R} - \hat{P}_1\,\hat{P}_0 \tag{16}$$

The large sample properties of the above estimates of $P_{10}(u)$ and $m_{10}(u)$ are considered in Brillinger (1976), where it is shown that the estimates (14) and (15) of the product density and cross-intensity are approximately *Poisson random variables*, which can be approximated by the two normal distributions $\mathrm{N}\{P_{10}(u),\ P_{10}(u)/b\ \mathrm{R}\}$ and $\mathrm{N}\{m_{10}(u),\ m_{10}(u)/b\,P_1\}$, respectively. $\mathrm{N}\{A, B\}$ refers to a normal distribution with mean A and variance B. In both cases, the variance of the estimate depends on the value of the parameter being estimated. In such cases it is usual to apply a variance stabilising transform (Kendall and Stuart, 1966; Jenkins and Watts, 1968). Brillinger (1976) proposes a square root transformation giving

$$\hat{P}_{10}(u)^{1/2} \approx \mathrm{N}\left\{P_{10}(u)^{1/2}, (4b\mathrm{R})^{-1}\right\} \tag{17}$$

$$\hat{m}_{10}(u)^{1/2} \approx \mathrm{N}\left\{m_{10}(u)^{1/2}, \left(4b N_0(\mathrm{R})\right)^{-1}\right\} \tag{18}$$

These parameter estimates have constant variance, which allows us to set *confidence limits* to test the hypothesis of independent (uncorrelated) spike trains. These confidence limits can be set in the following manner. Given an estimate $\hat{z}$ of a parameter z, which is approximately normally distributed with variance $\mathrm{var}\{\hat{z}\}$, then 95% confidence limits can be set at $\pm 1.96\left(\mathrm{var}\{\hat{z}\}\right)^{1/2}$. The asymptotic values for $(\hat{P}_{10}(u))^{1/2}$ and $(\hat{m}_{10}(u))^{1/2}$ for large u can be estimated using equations (7) and (5), and indicate the expected values for two independent spike trains. Therefore we have the following asymptotic distribution and 95% confidence limits for $(\hat{P}_{10}(u))^{1/2}$

$$\left(\hat{P}_1\,\hat{P}_0\right)^{1/2} \pm 1.96(4b\mathrm{R})^{-1/2} \tag{19}$$

and for $\left(\hat{m}_{10}(u)\right)^{1/2}$

$$\left(\hat{P}_1\right)^{1/2} \pm 1.96\left(4b N_0(\mathrm{R})\right)^{-1/2} \tag{20}$$

Estimated values lying inside the upper and lower confidence limits can be interpreted as evidence of uncorrelated spike trains.

The asymptotic distribution of the estimated cumulant density, $\hat{q}_{10}(u)$, is discussed in Rigas (1983), and can be approximated by

$$\mathrm{var}\{\hat{q}_{10}(u)\} \approx \frac{2\pi}{\mathrm{R}} \int_{-\pi/b}^{\pi/b} f_{11}(\lambda)\, f_{00}(\lambda)\, d\lambda \tag{21}$$

where $f_{11}(\lambda)$ and $f_{00}(\lambda)$ are the auto-spectra of processes N_1 and N_0, respectively. The auto-spectra of spike train data will be discussed below, however, under the assumptions of Poisson spike trains the variance in (21) can be approximated by $\left(P_1\, P_0 / \mathrm{R}b\right)$. For two independent spike trains, an asymptotic value and upper and lower confidence limit for the estimate of $\hat{q}_{10}(u)$ given in (16) can be set at

$$0 \pm 1.96\left(\hat{P}_1\, \hat{P}_0 / \mathrm{R}b\right)^{1/2} \tag{22}$$

It is worth pointing out that once the cross-correlation histogram, $\mathrm{J}_{10}^{\mathrm{R}}(u)$, has been obtained, the product density, cross-intensity and cumulant density can be estimated very easily, and confidence limits which depend only on the quantities b, R, N_0(R) and N_1(R), and not on the characteristics of the spike trains (other than the mean rates), can easily be determined.

Results

Example 1: Time Domain Point Process Parameter Estimates

We illustrate the application of the above point process parameters with a sample analysis of a pair of motor unit spike trains, recorded from the middle finger portion of the extensor digitorum communis (EDC) muscle of a normal healthy subject during a maintained postural contraction. The two spike trains contain 1293 and 919 spikes, the record duration is 100 seconds, sampled at 1 ms intervals. The first order statistics are N_0(R) = 1293, N_1(R) = 919, R = 100,000, $\hat{P}_0 = 0.01293$, $\hat{P}_1 = 0.00919$, and in addition $(\hat{P}_0 \hat{P}_1)^{1/2} = 0.0109$ and $\hat{P}_1^{1/2} = 0.096$. Shown in Fig. 1 are estimates of (A) the cross-correlation histogram, $\mathrm{J}_{10}^{\mathrm{R}}(u)$, (B) the square root of the product density, $(\hat{P}_{10}(u))^{1/2}$, (C) the square root of the cross-intensity function, $\hat{m}_{10}(u)^{1/2}$, and (D) the cumulant density function, $\hat{q}_{10}(u)$. All parameters have a bin width b=1.0, giving estimates with the same resolution as the sampled spike trains (1 ms). The relationship between the cross-correlation histogram and the other three parameter estimates, made explicit by equations (13) to (16), is clearly demonstrated in this figure. The three parameter estimates all have the same basic shape determined from the cross-correlation histogram. The main difference is in the asymptotic value of the three estimates, which reflect the different probability descriptions given in equations (4), (6) and (9). The asymptotic values and upper and lower confidence limits are 0.0109±0.0031 for $\hat{P}_{10}(u)^{1/2}$, 0.096±0.027 for $\hat{m}_{10}(u)^{1/2}$, and 0±6.7×10^{-5} for $\hat{q}_{10}(u)$. The main feature is the large peak at lag u=+5 ms, which exceeds the upper confidence limit in all three parameter estimates, indicating correlated motor unit activity. Also present in the cross-correlation histogram in Fig. 1A are smaller oscillatory features on either side of the central peak, these features are often referred to as sidebands and taken to reflect the presence of common rhythmic inputs to the two motoneurons whose motor unit activity is being studied (Moore et al., 1970). The confidence limits in the three parameter estimates indicate that these features are only of marginal significance at the 5% level. These features will be further discussed

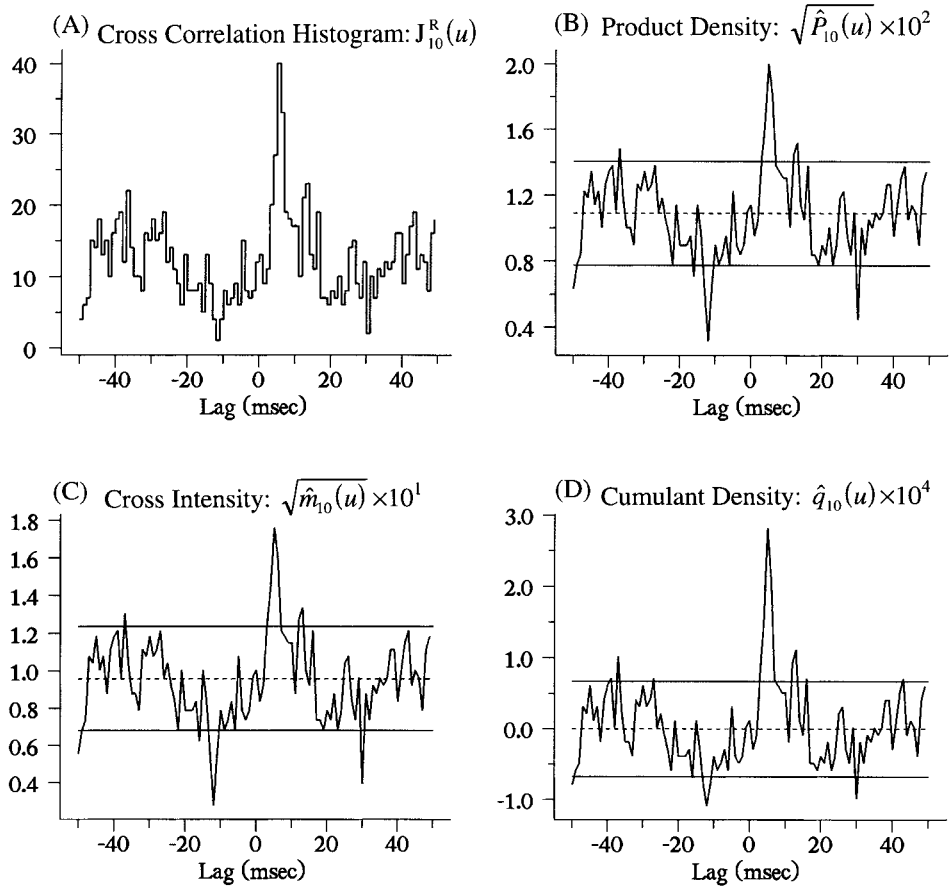

Fig. 1. Time domain analysis of the correlation between two motor unit spike trains. Estimates of (A) Cross-correlation histogram, $J_{10}^{R}(u)$, which has the units of counts, (B) square root of the product density, $(\hat{P}_{10}(u))^{1/2}\times10^{2}$, (C) square root of the cross-intensity function, $(\hat{m}_{10}(u))^{1/2}\times10^{1}$, and (D) cumulant density function, $\hat{q}_{10}(u)\times10^{4}$. Estimates have a bin width of b=1.0, and N_0(R)= 1293, N_1(R)=919, R=100,000. The dashed horizontal lines in B, C and D are the estimated asymptotic values, the solid horizontal lines are the estimated upper and lower 95% confidence limits under the assumption of independence.

below, with respect to frequency domain analysis, which is illustrated in Fig. 3. For uncorrelated spike trains, the three parameter estimates, $\hat{P}_{10}(u)^{1/2}$, $\hat{m}_{10}(u)^{1/2}$, and $\hat{q}_{10}(u)$, will fluctuate about their respective asymptotic values, the expected range of fluctuations can be estimated from the upper and lower confidence limits. Any significant departure outside these values, as in the peak at u=+5 ms in Fig. 1, can be taken to indicate a significant dependency between the spike trains at that particular lag value. Figure 1 illustrates the advantages of including confidence limits by focusing quickly on significant features in parameter estimates. The two parameter estimates $\hat{P}_{10}(u)^{1/2}$ and $\hat{m}_{10}(u)^{1/2}$ contain information about firing rates in their asymptotic distributions related to the probability descriptions in previous section. However, unless this is of specific interest, the presence of a statistically significant correlation can be inferred from any of the three estimates. In such situations, only one of the parameter estimates needs to be constructed, and the use of cumulant density estimates has the added advantage of being easily incorporated into the unified Fourier based framework presented below for dealing with spike train and/or time series data.

Part 2: Frequency Domain Analysis

The Finite Fourier Transform of Point Process and Time Series Data

All frequency domain analyses described below are based on parameter estimates formed from arithmetic combinations of *finite Fourier transforms*. The finite Fourier transform is therefore central to this analysis. This section defines and discusses how to estimate the finite Fourier transform of spike train and regularly sampled waveform data. Spike trains are assumed to be realizations of stochastic point processes, and waveform data are assumed to be realizations of time series. Point process data are assumed to meet the assumptions of orderliness discussed above, and time series data are assumed to be zero mean. Both types of data are further assumed to satisfy the two conditions of weak stationarity and a mixing condition. Weak stationarity implies that parameters which characterize a stretch of data do not change with time. The mixing condition implies that point process differential increments and/or time series sample values which are widely separated in time are independent. These assumptions are discussed in Halliday et al. (1995a). Both time series and point process data can be considered as belonging to the class of *stationary interval functions* considered in Brillinger (1972). The finite Fourier transform of a segment of point process N_1 containing T differential increments is defined as (Brillinger, 1972; Rosenberg et al., 1989)

$$d_{N_1}^{\mathrm{T}}(\lambda) = \int_0^{\mathrm{T}} e^{-i\lambda t}\, dN_1(t) \tag{23}$$

The integral in equation (23) can be thought of in a heuristic sense as comparing the periodicities of the sinusoids and cosinusoids of the complex Fourier exponential with the spacing between the spikes of process N_1, which allows information about periodic components in the spike train to be extracted. Modern spectral analysis methods invariably use a *fast Fourier transform* (FFT) algorithm to compute the finite Fourier transform of a sequence of data, at an equispaced set of Fourier frequencies. This requires equally spaced samples as input, which is achieved through the use of the differential increments to represent the point process N_1 in (23). Therefore, to estimate the quantity $d_{N_1}^{\mathrm{T}}(\lambda_k)$, using an FFT of length T we can approximate the integral in equation (23) by a discrete summation as (Brillinger, 1972; Rosenberg et al., 1982, 1989, Halliday et al., 1992)

$$d_{N_1}^{\mathrm{T}}(\lambda_j) \approx \sum_{t=0}^{\mathrm{T}-1} e^{-i\lambda_j t}\, dN_1(t) = \sum_{t=0}^{\mathrm{T}-1} e^{-i\lambda_j t} \left[N_1(t+\Delta t) - N_1(t)\right] \tag{24}$$

where τ_n are the times of occurrence of the N_1 events in the interval (0,T]. Since the point process is assumed orderly, the differential increments will have the value 0 or 1. The use of differential increments in equation (24) is therefore equivalent to representing the point process N_1 as a regularly sampled 0–1 time series. The Fourier frequencies, λ_j, are given by $\lambda_j = 2\pi j / T$, for j=0,…T/2. This defines a range for λ_j of (0, π), where π corresponds to the *Nyquist frequency* (cf. Chapter 45). The Fourier frequencies can be expressed in Hz as $j / \mathrm{T}\Delta t$, where T is the number of points in the finite Fourier transform, and Δt the sampling interval (seconds). The quantity $1 / \mathrm{T}\Delta t$ represents the fundamental Fourier frequency in cycles/s, i.e. the lowest frequency which can be resolved of 1 complete cycle of duration T, and represents the minimum spectral resolution of any parameters formed from $d_{N_1}^{\mathrm{T}}(\lambda_j)$.

In a similar fashion to (23), the Fourier transform of a segment of length T from a time series, x, is written as (Brillinger 1972, 1974)

$$d_x^{\mathrm{T}}(\lambda) = \int_0^{\mathrm{T}} e^{-i\lambda t}\, x(t)\, dt \tag{25}$$

Since $x(t)$ is a regularly sampled waveform, the sampled values can be readily evaluated by an FFT algorithm

$$d_x^{\mathrm{T}}(\lambda_j) \approx \sum_{t=0}^{\mathrm{T}-1} e^{-i\lambda_j t} x_t \tag{26}$$

where x_t are the sample values of $x(t)$ at time t. The Fourier frequencies, λ_j, are defined as for (24). Equation (26) performs a Fourier decomposition of the segment of $x(t)$ into constituent frequency components, which highlights distinct periodic components in the data (Brillinger, 1983).

Efficient FFT routines can be found in Bloomfield (1976, Chapter 4), Sorensen et al. (1987), and in the compendium of numerical methods by Press et al. (1989) which are available in a number of programming languages.

Definition and Estimation of Second Order Spectra

In this section we discuss the construction of estimates of second order spectra based on complex products of the finite Fourier transforms of point process and time series data discussed above. Following Halliday et al. (1995a) we use the term *hybrid* to characterize a parameter that depends on a time series and a point process. The auto-spectrum of time series x is denoted by $f_{xx}(\lambda)$, and of point process N_1 by $f_{11}(\lambda)$. The hybrid cross-spectrum between the two processes is denoted by $f_{x1}(\lambda)$. The asymptotic distribution of the finite Fourier transform for a broad variety of stationary processes, called "stationary interval functions" which include stationary time series and stationary point process data, is discussed in Brillinger (1972), where it is shown that for $\mathrm{T} \to \infty$, the asymptotic distribution of $d_{N_1}^{\mathrm{T}}(\lambda)$ and $d_x^{\mathrm{T}}(\lambda)$ is a complex normal. In the case of a times series x, this leads to consideration of the following statistic as an *estimate of the auto-spectrum*

$$\frac{1}{2\pi \mathrm{T}} \left| d_x^{\mathrm{T}}(\lambda) \right|^2 \tag{27}$$

This quantity, which is often referred to as the *periodogram*, $I_{xx}^{\mathrm{T}}(\lambda)$, was first proposed by Schuster (1898) to search for hidden periodicities in a series, x. The periodogram is not a consistent estimate of the spectrum $f_{xx}(\lambda)$, and requires further smoothing. One method to achieve this is averaging periodograms based on disjoint sections of data. Such an approach leads to

$$\hat{f}_{xx}(\lambda_j) = \frac{1}{2\pi \mathrm{LT}} \sum_{l=1}^{\mathrm{L}} \left| d_x^{\mathrm{T}}(\lambda_j, l) \right|^2 \tag{28}$$

as an estimate of the auto-spectrum of series x, at the Fourier frequencies λ_j defined above. Using this procedure involves splitting the complete record of R samples into L non-overlapping disjoint sections of length T, the quantity $d_x^{\mathrm{T}}(\lambda_j, l)$ refers to the finite Fourier transform of the l^{th} segment (l=1,…,L). An estimate of the auto-spectrum of the point process N_1, $\hat{f}_{11}(\lambda)$, is obtained by replacing $d_x^{\mathrm{T}}(\lambda_j, l)$ with $d_{N_1}^{\mathrm{T}}(\lambda_j, l)$ in equation (28). Using this approach, the *hybrid cross-spectrum* between N_1 and x, $\hat{f}_{x1}(\lambda)$ can be estimated as

$$\hat{f}_{x1}(\lambda_j) = \frac{1}{2\pi \mathrm{LT}} \sum_{l=1}^{\mathrm{L}} d_x^{\mathrm{T}}(\lambda_j, l)\, \overline{d_{N_1}^{\mathrm{T}}(\lambda_j, l)} \tag{29}$$

Cross-spectra between two time series and between two point processes can be estimated in a similar manner by substitution of the appropriate finite Fourier transforms into equation (29). The approach of smoothing periodograms is a widely used method of spectral estimation (Bartlett, 1948; Brillinger 1972; 1981; Rosenberg et al., 1989; Halliday et al., 1995a).

For large T and $\lambda \neq 0$, the estimated cross-spectrum $\hat{f}_{x1}(\lambda_j)$ may be seen to have the same form as a complex covariance parameter, $\mathrm{cov}\{A,B\} = E\{(A-E\{A\})\,\overline{(B-E\{B\})}\}$, and can be interpreted as the covariance between the components of processes N_1 and x at each Fourier frequency λ_j. The estimated auto-spectra, $\hat{f}_{11}(\lambda_j)$ and $\hat{f}_{xx}(\lambda_j)$, have the same form as a variance parameter which provides a measure of the variance (or power) at each Fourier frequency λ_j of the process x (Tukey, 1961). Other methods of estimating spectra of spike train data are discussed in Halliday et al. (1992).

Second order spectra can also be defined in terms of the Fourier transform of the appropriate auto- or cross-covariance (cumulant density) functions. For example, the spectrum of x can be defined as (Jenkins and Watts, 1968; Brillinger, 1981)

$$f_{xx}(\lambda) = \frac{1}{2\pi} \int_{-\infty}^{\infty} q_{xx}(u)\, e^{-i\lambda u}\, du \tag{30}$$

where $q_{xx}(u)$ is the auto-covariance or cumulant density of process x. In the point process case the expression becomes (Bartlett, 1963)

$$f_{11}(\lambda) = \frac{P_1}{2\pi} + \frac{1}{2\pi} \int_{-\infty}^{\infty} q_{11}(u)\, e^{-i\lambda u}\, du \tag{31}$$

where the additional term arises from the inclusion of the Dirac delta function in the definition of the auto-covariance (10). For u large $q_{11}(u)$ will tend to zero, which gives the asymptotic distribution of $f_{11}(\lambda)$ as $\lim_{\lambda \to \infty} f_{11}(\lambda) = P_1 / 2\pi$. This approximation is used above in the derivation of (22) from (21) with respect to the estimation of the variance of point process cumulant density functions. For the hybrid cross-spectrum, $f_{x1}(\lambda)$, the appropriate expression is

$$f_{x1}(\lambda) = \frac{1}{2\pi} \int_{-\infty}^{\infty} q_{x1}(u)\, e^{-i\lambda u}\, du \tag{32}$$

Other cross-spectra can be defined in a similar fashion. Equations (30) to (32) show the close relationship between cumulant density (covariance) functions and spectra. These relationships also show that it is possible to estimate spectra indirectly through the Fourier transform of covariance functions. Such an approach formed the basis of the first major practical digital time series analysis (Blackman and Tukey, 1958), before the advent of the FFT. Modern methods of spectral estimation generally use direct procedures based on FFT algorithms to estimate the finite Fourier transforms, as described above.

For estimates of the auto-spectrum, $\hat{f}_{xx}(\lambda)$, obtained via (28), it can be shown that the variance can be approximated by $\mathrm{var}\{\hat{f}_{xx}(\lambda)\} \approx \mathrm{L}^{-1}(f_{xx}(\lambda))^2$ (Brillinger 1972, 1981; Bloomfield, 1976), where L is the number of disjoint sections used to estimate the spectrum. This expression contains the value of the actual spectrum at a particular frequency and will therefore change with changing frequency. The appropriate variance stabilising transform is the natural log, giving $\mathrm{var}\{\ln(\hat{f}_{xx}(\lambda))\} \approx \mathrm{L}^{-1}$. It is customary practice to plot spectra on a $\log_{10}$ scale, thus

$$\mathrm{var}\left\{\log_{10}\left(\hat{f}_{xx}(\lambda)\right)\right\} = \left(\log_{10}(\mathrm{e})\right)^2\, \mathrm{L}^{-1} \tag{33}$$

with a resulting estimate and 95% confidence limits at frequency λ of

$$\log_{10}\left(\hat{f}_{xx}(\lambda)\right) \pm 0.851\, \mathrm{L}^{-1/2} \tag{34}$$

An alternative method of indicating the confidence limit, which is independent of the value of the spectrum, is to plot a scale bar of magnitude $\left(1.7\,L^{-1/2}\right)$ as a guide to interpret any distinct features in the estimated spectrum. In the point process case, where the spectra have an asymptotic value, the three lines

$$\log_{10}\left(\frac{\hat{P}_1}{2\pi}\right), \quad \log_{10}\left(\frac{\hat{P}_1}{2\pi}\right) \pm 0.851\,L^{-1/2} \tag{35}$$

can be used as a guide to interpret features in the estimate of $\hat{f}_{11}(\lambda)$.

Results: Auto-Spectra

In Fig. 2 are shown examples of auto-spectral estimates of both point process and time series signals. All these estimates have been constructed from data sampled at 1 ms ($\Delta t = 10^{-3}$ s), and a segment length of 1024 points (T=1024) in the finite Fourier transforms (24) and (26), giving a spectral resolution of 0.977 Hz.

Example 2: Motor Unit Spectrum

Figures 2A and 2B are from the same data set as analysed in Fig. 1. This data consists of two individual motor unit discharges recorded from the middle finger portion of the (EDC) muscle in a human subject, and the tremor recorded simultaneously from the distal phalanx of the finger using an accelerometer, while the subject maintained the unrestrained middle finger extended in a horizontal position (see Conway et al., 1995b and Halliday et al., 1995a, for further details of the experimental protocol). The duration of the data set is 100 seconds (R=10^5), giving L=97 for this data set. The spike train whose spectral estimate is illustrated in Fig 2A, N_0, has 1293 spikes (N_0(R)=1293), a mean rate of 12.9 spikes/s, and the coefficient of variation (c.o.v.) is 0.17. For the tremor signal the mean RMS value is 6.91 cm/s^2. The dominant feature of the log plot of the motor unit spectrum is the large peak around 13 Hz, corresponding to the mean rate of firing, illustrating that the mean firing rate is the dominant rhythmic component in this motor unit discharge. There is a less well-defined peak centered around 26 Hz, this frequency matches the expected first harmonic of the spectral peak corresponding to the mean discharge rate. At higher frequencies the estimate lies almost entirely inside the expected upper and lower 95% confidence intervals shown as the solid horizontal lines. These intervals are constructed under the assumption of a random (Poisson) spike train, and at higher frequencies this motor unit discharge behaves as a random spike train. This behavior is a consequence of the mixing condition discussed above, where differential increments widely separated in time tend to become independent (a characteristic of Poisson spike trains). At lower frequencies, however, the spectrum of this spike train exhibits significant departure from that expected for a Poisson spike train. For spike trains whose dominant spectral component reflects the mean firing rate, the appearance of harmonic components in their spectral estimates is related to the c.o.v. A more regular discharge generally has a spectral estimate which contains more harmonic components.

Example 3: Tremor Spectrum

The log plot of the estimated tremor spectrum, $\hat{f}_{xx}(\lambda)$, in Fig. 2B has a peak around 21 Hz, this is the dominant component of physiological tremor recorded from the unrestrained finger, and is due in part to the natural resonance of the extended finger. For a

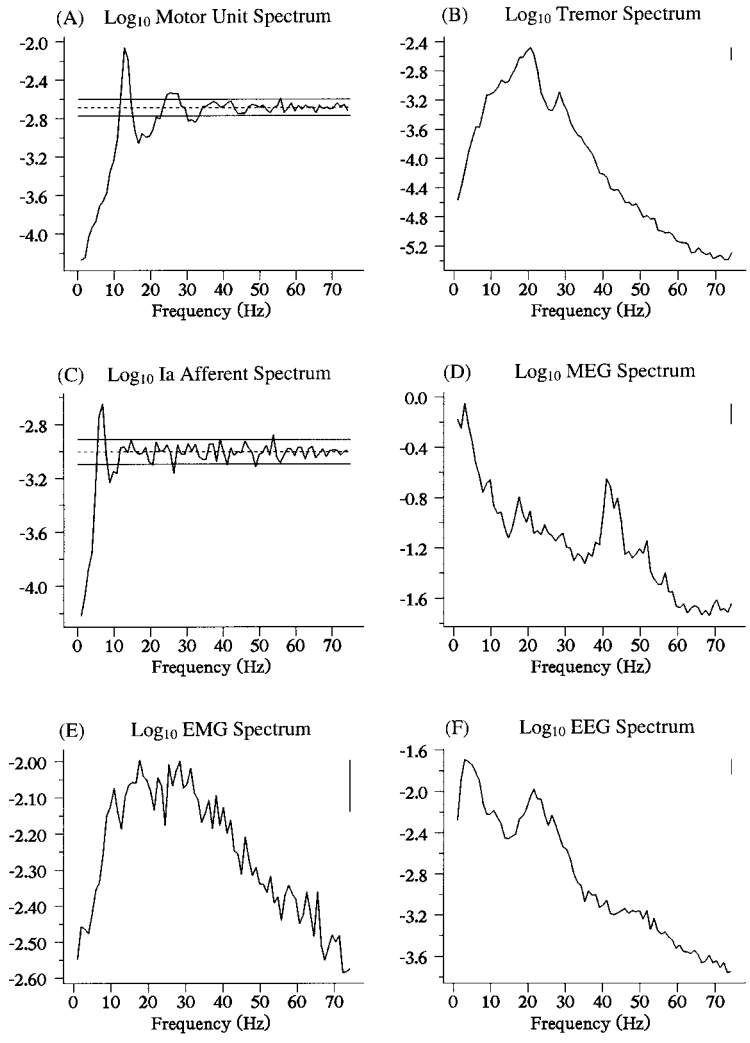

Fig. 2. Examples of spectral estimates. Log plots of estimated power spectra for (A) motor unit spike train during position holding of the extended middle finger, and (B) simultaneous tremor acceleration signal, (C) Ia afferent spike train, (D) Magnetoencephalogram recorded over the sensorimotor cortex, (E) rectified surface EMG from wrist extensors during maintained wrist extension, and (F) simultaneous EEG recorded over the sensorimotor cortex. Dashed horizontal lines in (A, C) represent the asymptotic value of each estimate, solid horizontal lines give the estimated upper and lower 95% confidence limits, based on the assumption of a Poisson spike train. Solid vertical lines at the top right in (B, D, E, F) give the estimated magnitude of a 95% confidence interval for each spectral estimate. For all data the sampling interval Δt=1 ms, and for all estimates T=1024 points.

more detailed discussion of the spectrum of physiological tremor see Stiles and Randall, (1967) and Halliday et al. (1995a). There is another smaller peak around 28 Hz. The confidence interval for the spectral estimate can be used as a guide to help establish if this smaller peak is significant. The confidence interval is shown as the solid vertical line in the top right of Fig. 2B, of magnitude 0.173 dB. This is the same as the spacing between the upper and lower confidence limits (solid lines) in Fig. 2A, estimated from the same number of segments (see equations (34) and (35) above). Comparison of the local fluctuation around 28 Hz with the scale bar suggests that this localised peak in the spectrum

does reflect a distinct rhythmic component as opposed to chance fluctuations in the spectral estimate, which we would expect to be of a magnitude smaller than this scale bar. The correlation between the single motor unit discharge in Fig. 2A and this tremor signal is examined below in Fig. 4.

Example 4: Ia Afferent Spectrum

In Fig. 2C is shown another point-process spectral estimate, this is for a single Ia afferent discharge recorded using the microneurography technique (Vallbo and Hagbarth, 1968) from a human subject during low force voluntary isometric contraction of the fourth finger portion of the EDC muscle (for further details see Halliday et al., 1995b). The data is 89 seconds in duration (R=89,000; L=86), and contains 553 spikes. The mean rate is 6.2 spikes/s, and the c.o.v. is 0.21. The log plot of this spectral estimate contains a clear peak around 6 Hz, reflecting the mean firing rate of the Ia.

Example 5: MEG Spectrum

The spectral estimate in Fig. 2D is for human cortical activity, in this case recorded as the *magnetoencephalogram* (MEG; cf. Chapter 37) over the sensorimotor cortex during a maintained contraction of a contralateral intrinsic hand muscle (for details, see Conway et al., 1995a). This spectral estimate, which is for a record of 110 seconds (R= 110,000; L=107), has most power present at lower frequencies, with decreasing power at higher frequencies. Comparison of local fluctuations in this estimate with the 95% confidence interval (top right) indicates distinct rhythmic components centered about 18 and 42 Hz, the latter is particularly distinct. The functional significance of these rhythms is discussed in Conway et al. (1995a).

Example 6: EMG and EEG Spectra

The two spectral estimates illustrated in Fig. 2E and F are for a simultaneously recorded surface *electromyogram* (EMG; cf. Chapter 26) from the wrist extensors and a bipolar *electroencephalogram* (EEG; cf. Chapter 35) from over the contralateral sensorimotor cortex in a human subject during maintained wrist extension (for details see Halliday et al., 1998). These spectra are estimated from a total of 138 seconds of data. The log plot of the EMG spectrum is for the rectified surface EMG signal, and exhibits a broad peak from around 10 to 40 Hz. The reason for analysing rectified EMG is discussed in Example 9 (in connection with Fig. 5). The EEG spectral estimate has a concentration of power at low frequencies (the decrease at the lowest frequencies reflects the high-pass filtering of 3 Hz associated with the instrumentation), and a clearly defined peak centered around 22 Hz. The 95% confidence intervals have the same magnitude for both estimates. The correlation between these two signals is examined below in Fig. 5. It is interesting to compare this EEG spectral estimate to the MEG spectral estimate (Fig. 2D), recorded from a similar location in a different subject (see discussion in Halliday et al., 1998).

The above six spectral estimates illustrate analysis of a broad range of signal types, which are typical of those encountered in neurophysiological experiments. The next part discusses how the correlation between pairs of such signals can be investigated. The starting point for these analyses are estimates of the auto-spectra of individual signals, and cross-spectra between pairs of signals.

Part 3: Correlation Between Signals

Within the present framework the dependence between two signals can be characterized by parameters which assess the correlation between the signals. In the frequency domain it is customary to consider the magnitude squared of the correlation between the Fourier transforms of the two signals under consideration. For the bivariate point processes (N_0, N_1) this leads to (Brillinger 1975; Rosenberg et al., 1989)

$$\lim_{T\to\infty} \left|\mathrm{corr}\left\{d_{N_1}^{T}(\lambda), d_{N_0}^{T}(\lambda)\right\}\right|^2 \tag{36}$$

as a measure of the correlation between processes N_0 and N_1. This quantity is called the *coherence function* (Wiener, 1930), denoted by $|R_{10}(\lambda)|^2$, estimates of which provide a measure of the strength of correlation between N_0 and N_1 as a function of frequency. The definition of the correlation $\mathrm{corr}\{d_{N_1}^{T}(\lambda), d_{N_0}^{T}(\lambda)\}$ between the Fourier transforms of the two point processes N_0 and N_1 in terms of variance and covariance, given by the expression: $\mathrm{corr}\left\{d_{N_1}^{T}(\lambda), d_{N_0}^{T}(\lambda)\right\} = \mathrm{cov}\left\{d_{N_1}^{T}(\lambda), d_{N_0}^{T}(\lambda)\right\} \Big/ \sqrt{\mathrm{var}\left\{d_{N_1}^{T}(\lambda)\right\}\mathrm{var}\left\{d_{N_0}^{T}(\lambda)\right\}}$, leads to the alternative definition for the coherence function between point processes N_0 and N_1 as

$$|R_{10}(\lambda)|^2 = \frac{|f_{10}(\lambda)|^2}{f_{11}(\lambda) f_{00}(\lambda)} \tag{37}$$

Coherence functions provide a normative measure of linear association between two processes on a scale from 0 to 1, with 0 occurring in the case of independent processes (Brillinger, 1975; Rosenberg et al., 1989). Expression (37) leads to an estimation procedure by substitution of the appropriate spectral estimates to give

$$|\hat{R}_{10}(\lambda)|^2 = \frac{|\hat{f}_{10}(\lambda)|^2}{\hat{f}_{11}(\lambda)\hat{f}_{00}(\lambda)} \tag{38}$$

where $|\hat{R}_{10}(\lambda)|^2$ denotes an estimate of $|R_{10}(\lambda)|^2$. A similar procedure can be used to estimate the coherence between a time series x and point process N_1

$$|\hat{R}_{x1}(\lambda)|^2 = \frac{|\hat{f}_{x1}(\lambda)|^2}{\hat{f}_{xx}(\lambda)\hat{f}_{11}(\lambda)} \tag{39}$$

and the coherence between two time series x and y, $|R_{xy}(\lambda)|^2$, can be estimated in a similar manner. Estimates of the necessary second order spectra can be constructed using the method of disjoint sections outlined above in Part 2. Coherence estimates obtained in this way all have the same large sample properties for any combination of point process and/or time series data (Halliday, 1995a). A confidence interval at the 100α% point which is based on the assumption of independence, i.e. $|R_{x1}(\lambda)|^2 = 0$, is given by the value $1-(1-\alpha)^{1/(L-1)}$, where L is the number of disjoint sections used to estimate the second order spectra (Bloomfield, 1976; Brillinger, 1981). Therefore an upper 95% confidence limit can be set at the constant level

$$1-(0.05)^{1/(L-1)} \tag{40}$$

and estimated values of coherence below this level can be taken as evidence for a lack of correlation between the two processes at a particular frequency. The setting of confi-

dence limits about the estimated values of coherence when significant correlation is present is discussed in Halliday et al. (1995a).

Coherence estimates assess the magnitude of correlation between two signals in the frequency domain. Information relating to timing can be obtained by examining the phase difference between the two signals. For point process N_1 time and series x, the *phase spectrum*, $\Phi_{x1}(\lambda)$, is defined as the argument of the cross-spectrum

$$\Phi_{x1}(\lambda) = \arg\{f_{x1}(\lambda)\} \tag{41}$$

This function can be estimated by direct substitution of the estimated cross-spectrum, equation (29) as

$$\hat{\Phi}_{x1}(\lambda) = \arg\{\hat{f}_{x1}(\lambda)\} \tag{42}$$

Phase spectra between other combinations of point-process and/or time series data can be defined and estimated in similar fashion. Phase estimates are only valid when there is significant correlation between the two signals. In practice $|\hat{R}_{x1}(\lambda)|^2$ can be used to indicate the regions where $\hat{\Phi}_{x1}(\lambda)$ has a valid interpretation. Phase estimates can be interpreted as the phase difference between harmonics of N_1 and x at frequency λ. The arctan function can be used to obtain the argument of the cross-spectrum, resulting in a phase estimate over the range $[-\pi/2, \pi/2]$ radians. However, the signs of the real and imaginary parts of $\hat{f}_{x1}(\lambda)$ can be used to determine in which quadrant the arctangent falls, so extending the range to $[-\pi, \pi]$ radians.

Phase estimates can often be interpreted according to different theoretical models. A useful model is the phase curve for two signals which are correlated with a fixed time delay, where the theoretical phase curve is a straight line, passing through the origin (0 radians at 0 frequency) with slope equal to the delay, and a positive slope for a phase lead, and negative slope for a phase lag (see Jenkins and Watts, 1968). In situations where there is significant correlation over a wide range of frequencies and a delay between two signals, it is reasonable to extend the phase estimate outside the range $[-\pi, \pi]$ radians, which avoids discontinuities in phase estimates. Such a phase estimate is often referred to as an *unconstrained phase estimate*. The representation of phase estimates is discussed in Brillinger (1981). Different theoretical phase curves for other forms of correlation structure are discussed in Jenkins and Watts (1968). Details for the construction of confidence limits about estimated phase values can be found in Halliday et al. (1995a). In situations where the correlation structure between two signals is dominated by a delay it is possible to estimate this delay from the phase curve, such an approach, based on weighted least squares regression, is described in the Appendix in Rosenberg et al. (1989). This method has the advantage of providing an estimate of the standard error for the estimated delay.

As discussed above, correlation analysis in neurophysiology has traditionally been performed in the time domain. We next discuss how correlation between point-process and/or time series data can be characterized as a function of time. Within the present Fourier based analytical, the correlation between two signals as a function of time can be estimated using *cumulant density functions*. These can be defined in terms of the *inverse Fourier transform of the cross-spectrum* (Jenkins and Watts, 1968; Brillinger, 1974). The second order hybrid cumulant density function between processes N_1 and x, $q_{x1}(u)$ is defined as

$$q_{x1}(u) = \int_{-\pi}^{\pi} f_{x1}(\lambda)\, e^{i\lambda u}\, d\lambda \tag{43}$$

This expression and equation (32) illustrate the equivalence between time and frequency domain analysis, cumulant densities and spectra form a Fourier transform pair, cf.

(30) and (32). The above hybrid cumulant can be estimated by the following expression

$$\hat{q}_{x1}(u) = \frac{2\pi}{\mathrm{T}} \sum_{|j| \le \mathrm{T}/2b} \hat{f}_{x1}(\lambda_j)\, e^{i\lambda_j u} \tag{44}$$

where $\lambda_j = 2\pi j/\mathrm{T}$ are the Fourier frequencies, and b is the desired time domain bin width ($b \ge 1.0$), a value of $b=1.0$ results in a time domain estimate with the same temporal resolution as the sampling rate of the two signals. Equation (44) can be implemented using a real valued inverse FFT algorithm (e.g. Sorensen et al., 1987). The point process cumulant density function $q_{10}(u)$ and the time series cumulant density function $q_{xy}(u)$ can be defined and estimated in terms of the appropriate cross-spectra, $f_{10}(\lambda)$ and $f_{xy}(\lambda)$, respectively, using equations (43) and (44).

Cumulant density functions can be interpreted as statistical parameters which provide a measure of linear dependence between two signals (Brillinger, 1972; Rosenblatt, 1983; Mendel, 1991). If the two signals are independent, the value of the cumulant is zero. Cumulant densities can assume either positive or negative values. Unlike coherence estimates, they are not bounded measure of association, therefore there is no upper limit indicating a perfect linear relationship. In the case of hybrid data, $\hat{q}_{x1}(u)$ has an interpretation similar to a spike triggered average (Rigas, 1983; Halliday et al., 1995a). The relationship between the point-process cumulant density and the cross-correlation histogram was discussed in Part 1. It is possible to define and estimate cumulant density functions directly in the time domain, however, estimation via the frequency domain using equation (44) provides a unified framework for dealing with different data types, and is necessary for the construction of confidence limits for cumulant density estimates.

The variance of the hybrid cumulant density estimate (44) based on the assumption of independent processes can be approximated by (Rigas, 1983)

$$\mathrm{var}\{\hat{q}_{x1}(u)\} \approx \frac{2\pi}{\mathrm{R}} \int_{-\pi/b}^{\pi/b} f_{xx}(\lambda)\, f_{11}(\lambda)\, d\lambda \tag{45}$$

where R is the record length, and b is the bin width of the estimate used in equation (44). This expression can be estimated using a discrete summation and substituting estimates of the spectra $f_{xx}(\lambda)$ and $f_{11}(\lambda)$ giving

$$\mathrm{var}\{\hat{q}_{x1}(u)\} \approx \left(\frac{2\pi}{\mathrm{R}}\right)\left(\frac{2\pi}{\mathrm{T}}\right) \sum_{j=1}^{(\mathrm{T}/2-1)/b} 2\, \hat{f}_{xx}(\lambda_j)\hat{f}_{11}(\lambda_j) \tag{46}$$

where $\lambda_j = 2\pi j/\mathrm{T}$, R is the record length, b the bin width, and T is the segment length used in the estimation of the finite Fourier transforms (24) and (26). Under the assumption of independent processes, the asymptotic value and upper and lower 95% confidence limits for the estimated cumulant (44) are given by

$$0 \pm 1.96\left[\left(\frac{2\pi}{\mathrm{R}}\right)\left(\frac{2\pi}{\mathrm{T}}\right) \sum_{j=1}^{(\mathrm{T}/2-1)/b} 2\, \hat{f}_{xx}(\lambda_j)\hat{f}_{11}(\lambda_j)\right]^{1/2} \tag{47}$$

Values of the estimated cumulant $\hat{q}_{x1}(u)$ lying inside the upper and lower 95% confidence limits can be taken as evidence of no linear correlation between point process N_1 and time series x at a particular value of lag u. Equations (45) to (47) are valid for cumulant density estimates constructed from other combinations of time series and/or point process data. For the point process cumulant density $\hat{q}_{10}(u)$, the assumption of Poisson spike trains allows the asymptotic values of the two point process spectra

$\lim_{\lambda\to\infty} f_{00}(\lambda) = P_0 / 2\pi$, and $\lim_{\lambda\to\infty} f_{11}(\lambda) = P_1 / 2\pi$ to be used to approximate the values of the spectra in (47), resulting in the simplified expression (22). This simplification allows confidence intervals for point process cumulants to be estimated without having to estimate the spectra. For the stochastic spike train discharges encountered in neurophysiological experiments this approximation results in estimated confidence intervals which plotted on a graph are almost indistinguishable from those obtained by integration of the spectra.

Equation (43) defines cumulant densities in terms of the inverse Fourier transform of the cross-spectrum, which leads to the estimation procedure in equation (44). It is also possible to define and estimate cumulant densities directly in the time domain. In the case of point process data this was done in Part 1. The interpretation of cumulant densities does not, in general, depend on the method of estimation.

For point process data, the derivation of cumulant densities directly in the time domain in terms of the correlation between differential increments is discussed in Brillinger (1975) and Rosenberg et al. (1989). For two point processes N_0 and N_1 the correlation between differential increments of the two point processes leads to the expression

$$\operatorname{corr}\{\mathrm{d}N_1(t+u), \mathrm{d}N_0(t)\} = q_{10}(u)\frac{\sqrt{du\,dt}}{\sqrt{P_1\,P_0}} \tag{48}$$

The term relating to the sampling interval in the differential increments, $\sqrt{du\,dt}$, illustrates the unbounded nature of cumulant density estimates. Other point process time domain measures of association, based on product density functions, are given in Brillinger (1975).

In the case of hybrid data, the spike triggered average between point process N_1 and time series x, which we denote by $\mu_{x1}(u)$, can be estimated as (Rosenberg et al., 1982; Rigas, 1983)

$$\hat{\mu}_{x1}(u) = \frac{1}{\mathrm{R}} \sum_{i=1}^{N_1(\mathrm{R})} x(\tau_i + u) \tag{49}$$

where R is the record length and τ_i are the times of the events in process N_1, (i= 1,…,N_1(R)). This estimate of the spike triggered average can be used to estimate the hybrid cumulant $\hat{q}_{x1}(u)$ as (Rosenberg et al., 1982; Rigas, 1983)

$$\hat{q}_{x1}(u) = \hat{\mu}_{x1}(u) - \hat{P}_1\,\hat{\mu}_x \tag{50}$$

where $\hat{P}_1$ is the estimated mean rate of process N_1, see (11), and $\hat{\mu}_x$ is the mean of process x. This equation illustrates the close relationship between the spike triggered average and the hybrid cumulant density; indeed, for a zero mean time series (which is a usual assumption for time series analysis) the two parameters are the same.

For zero mean time series data, $x(t)$ and $y(t)$, the cumulant density can be estimated for small lag u, as the *cross-covariance function* (Parzen, 1961; Bloomfield, 1976; Brillinger, 1981)

$$\hat{q}_{xy}(u) = \frac{1}{\mathrm{R}} \sum_{t=1}^{\mathrm{R}-|u|} x_{t+u}\, y_t \tag{51}$$

The use of a Fourier based estimation framework has advantages over the more traditional approach of estimating time domain parameters directly in the time domain. Firstly it provides a unified estimation procedure, both for constructing parameter estimates and for constructing confidence intervals. Equations (44) and (46) are valid for any pairwise combination of point process and/or time series data, thus the same soft-

ware routines can be used for all data types. The same is not true for direct time estimation in the time domain, as illustrated by the differences in equations (12) for point process data, (49) for hybrid data and (51) for time series data. As mentioned above the method of estimation does not affect the interpretation of parameter estimates. Cumulant densities can be interpreted as statistical parameters which provide a measure of dependence between point process and/or time series data. In the case of point process data the cumulant density is closely related to the more traditionally used cross-correlation histogram, and for a zero mean time series, the hybrid cumulant density is the same as the more traditionally used spike triggered average. The present report presents these parameters in the context of a unified Fourier based framework which can assess the correlation between signals in both the time domain and frequency domain – an approach which can offer extra insight into complex neural systems. The time and frequency domain parameters should be viewed as complementary to each other. Equations (32) and (43) illustrate the mathematical equivalence of cumulant density functions and second order spectra (via the Fourier transform). However, mathematical equivalence does not necessarily result in equivalence of representation, a point often made in the writings of J.W. Tukey (Tukey, 1980; see also Fig15, Rosenberg et al., 1989), and illustrated below in Fig. 3. Therefore both time and frequency domain parameters should routinely be used for data analysis.

The above Fourier based methods all involve an assumption of linearity, extension of these methods to higher-order analyses is described in Halliday et al. (1995a).

Results : Time and Frequency Domain Correlation Analyses

In this section we illustrate application of the parameters defined above to characterize the correlation between pairs of signals. This is done for four data sets which illustrate the analysis of different combinations of data: point process data, hybrid data (point process and time series) and time series data.

Example 7: Motor Unit – Motor Unit Coherence and Phase

The first example considers the same motor unit pair whose time domain analysis is illustrated in Fig. 1. The estimated cumulant density for this data set is illustrated in Fig. 1D, this is the direct time domain estimate, based on equation (16). The Fourier based estimate (equation (44), b=1.0, T=1024, L=97) is graphically indistinguishable from this. The upper and lower 95% confidence intervals in Fig. 1D are based on the simplified expression (22) and have the values $\pm 6.76\times10^{-5}$, those estimated by integration of the cumulant (47) have the values $\pm 6.73\times10^{-5}$. For the type of spike trains illustrated in this report, the simplified estimate for point process cumulant density confidence intervals provides almost identical values to those obtained by integration of the spectra. The simplified expression (22) will be useful for spike trains whose spectra only deviate from the asymptotic value for Poisson spike trains over a limited range of frequencies compared with the Nyquist frequency (500 Hz for this data). The estimated coherence, $\left|\hat{R}_{10}(\lambda)\right|^2$, and phase, $\hat{\Phi}_{10}(\lambda)$ (T=1024), for this data are shown in Fig. 3. The coherence between the two motor units, N_0 and N_1, has two distinct bands, from 1–6 Hz and 20–30 Hz. These frequency bands do not coincide with the peak in the spectrum of motor unit 0 (fig 2A) or motor unit 1 (not shown), thus we can conclude that the motor unit firing rate does not contribute to the coherence between this pair of motor units. The coherence estimate reflects periodic components present in the common inputs which are responsible for the synchronized motor unit firing (see Farmer et al., 1993 for

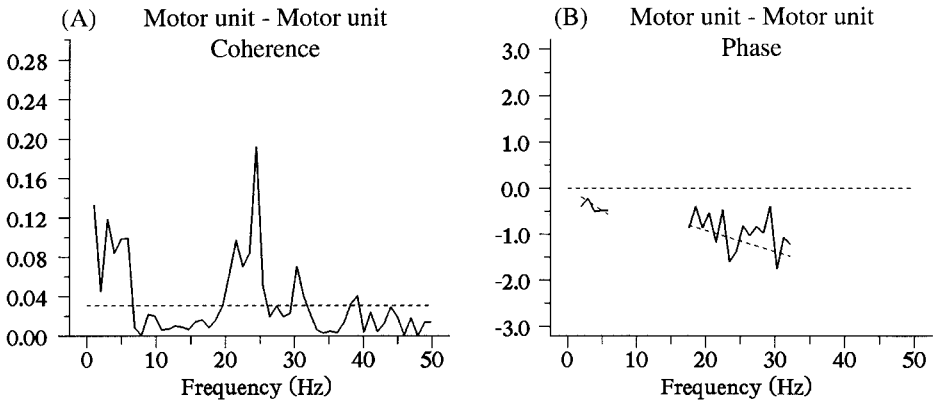

Fig. 3. Frequency domain analysis of motor unit correlation. Estimate of (A) coherence, $\left|\hat{R}_{10}(\lambda)\right|^2$, and (B) phase, $\hat{\Phi}_{10}(\lambda)$, between same motor unit data illustrated in Fig. 1. The horizontal dashed line in (A) gives the estimated upper 95% confidence limit based on the assumption of independence. The phase estimate in (B) is plotted where the coherence (A) is significant. The dotted lines through each section of the phase estimate are the theoretical phase curves for delays of 15.5 ms in the 1–6 Hz section, and 7.3 ms in the 18–32 Hz section (see text for details).

further discussion). The peak in the cumulant density estimate (Fig. 1D) indicates synchronized motor unit activity, the small sidebands which occur at around 40 ms on either side of the central peak further suggest a periodic component around 25 Hz is present, as indicated by the coherence estimate. However, comparison of Figs. 1D and 3A illustrates that different parameters can emphasize different features of the data – the cumulant estimate has sidebands which are only marginally significant, whereas the coherence estimate has a clear peak around 20–30 Hz – and argues in favor of both time and frequency domain analysis. The phase estimate is shown in Fig. 3B (solid lines), plotted in radians over the two regions where there is significant correlation between the motor units, estimated by inspection of the coherence estimate as 1–6 Hz and 18–32 Hz. In the time domain, the two motor units have a correlation structure which is dominated by a delay, as indicated by the peak at +5 ms in the cumulant (Fig. 1D). The phase estimate between the two motor units also reflects this delay, and the regression method described in the Appendix in Rosenberg et al. (1989) was used to estimate the slope of the phase curve in each section. These give delays of 15.5±3.6 ms for the delay in the 1–6 Hz section, and 7.3±1.2 ms in the 18–32 Hz section. The delay in the 18–32 Hz region corresponds with the latency estimated from the time to the peak in the cumulant, whereas the delay in the lower frequency range is longer. The cumulant estimate in Fig. 1D does have a smaller peak centered around +13 ms, which is consistent with the delay estimated from the phase over 1–6 Hz. To summarize, this example has examined the correlation between a pair of motor unit discharges, which exhibit a tendency for correlated firing dominated by a delay between the firing times and involving two distinct rhythmic components. The central peak in the cumulant density indicates synchronized firing, the maximum occurs at a latency of +5 ms, and small sidebands centered around 40 ms on either side suggest the presence of a rhythmicity around 25 Hz in the correlation. The frequency domain analysis reveals that the dominant component in the motor unit firing is the rhythmic component associated with the mean firing rate, that the motor units are coupled over two frequency bands, 1–6 and 18–32 Hz which do not correspond with the firing rate, and that different delays are associated with the coupling in each frequency band.

Example 8: Motor Unit – Tremor Coherence, Phase and Cumulant

The second example considers hybrid data, and examines the relationship between one of the motor unit discharges from the previous example and a simultaneously recorded tremor signal. The spectrum of the tremor signal is discussed above in Section 2.2, and is shown in Fig. 2B. Figure 4 illustrates the estimated coherence, $\left|\hat{R}_{x0}(\lambda)\right|^2$, phase, $\hat{\Phi}_{x0}(\lambda)$ (T=1024), and cumulant density, $\hat{q}_{x0}(u)$ (b=1.0), between the motor unit, N_0, and the tremor, x. The coherence estimate (Fig. 4A) has significant values over a broad range of frequencies, with evidence of two distinct bands which have maximum values around 6 Hz and 22 Hz. These correspond to the same frequency bands as the motor unit correlation, however, the magnitude of this coherence estimate is greater than that between the two motor units (see Conway et al., 1995b for further discussion). The phase estimate, Fig. 4B, in this example plotted in unrestrained form (see Part 3), has values which are constantly decreasing, however, the slope is not constant over the broad frequency range where the coherence is significant. Thus the pure delay model is not appropriate to explain this phase curve. The dominant feature in the hybrid cumulant den-

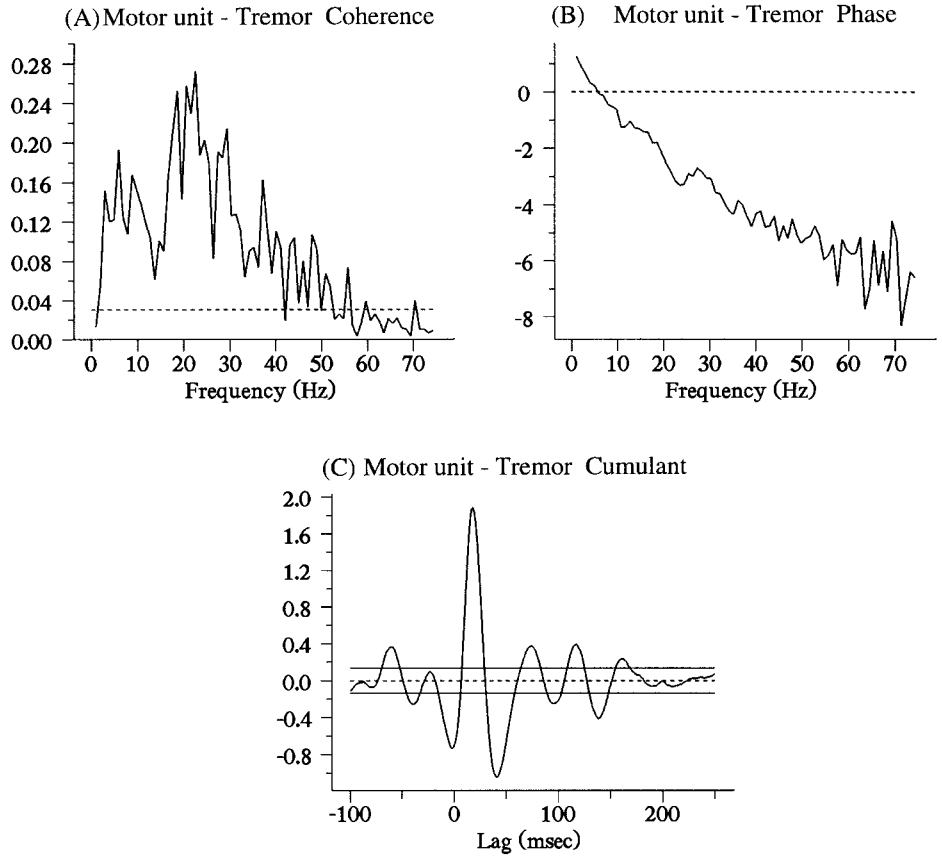

Fig. 4. Correlation between a single motor unit and a tremor acceleration signal. Estimate of (A) coherence, $\left|\hat{R}_{x0}(\lambda)\right|^2$, (B) phase, $\hat{\Phi}_{x0}(\lambda)$, and (C) cumulant density, $\hat{q}_{x0}(u)\times 10^4$, between one of the motor units illustrated in Figs. 1, 3 and a simultaneously recorded tremor acceleration signal. The horizontal dashed line in (A) gives the estimated upper 95% confidence limit based on the assumption of independence. The phase estimate in (B) is plotted in unrestrained form. The horizontal lines in (C) are the asymptotic value (dashed line at zero) and estimated upper and lower 95% confidence limits, based on the assumption of independence. The motor unit spectrum is illustrated in Fig. 2A, the tremor spectrum is shown in Fig. 2B.

sity estimate (Fig. 4C) is the large peak just after time zero, with a maximum around +17 ms. As discussed above, this cumulant can be interpreted as a spike triggered average, and provides an estimate of the acceleration response to motor unit impulses. It has a general form like a damped oscillation. A regression analysis on the part of the phase curve where the slope does pass through zero, from 11 Hz to 47 Hz, gives a delay of 17.9±0.7 ms, which matches well the peak value in the cumulant. An alternative interpretation of a similar data set, based on linear systems analysis, is described in Halliday et al. (1995a).

Example 9: EMG - EEG Correlation

The third example studies the correlation between two time series, namely the EEG and surface EMG signals whose auto-spectra are illustrated in Fig. 2E and 2F (see Part 1 and Halliday et al., 1998 for a description of the experimental protocol). Figure 5 illustrates the coherence, $\left|\hat{R}_{yx}(\lambda)\right|^2$, phase, $\hat{\Phi}_{yx}(\lambda)$ (T=1024) and cumulant density, $\hat{q}_{yx}(u)$ (b= 1.0), estimates between the EEG signal, x, and rectified surface EMG signal, y. The justification for using rectified surface EMG (without any smoothing) is that it reduces the components in the finite Fourier transform (26) which are due to the shape of individual muscle action potentials, while retaining information related to their spacing. This is further discussed in Halliday et al. (1995a).

In constructing the coherence and phase estimates shown in Fig. 5, the auto- and cross-spectral estimates have been further smoothed using a *Hanning filter*. This involves a weighted average of adjacent values in the frequency domain. If we denote the cross-spectral estimate between x and y with Hanning as $\hat{f}'_{yx}(\lambda_j)$, at frequency λ_j, this is obtained from the original estimate, based on (29), $\hat{f}_{yx}(\lambda_j)$ as

$$\hat{f}'_{yx}(\lambda_j) = \frac{1}{4}\hat{f}_{yx}(\lambda_{j-1}) + \frac{1}{2}\hat{f}_{yx}(\lambda_j) + \frac{1}{4}\hat{f}_{yx}(\lambda_{j+1}) \tag{52}$$

This procedure applies a moving average with weights $^1/_4$, $^1/_2$, $^1/_4$ to obtain the smoothed spectral estimates, which are then used to form coherence and phase estimates as described in Part 2. The use of smoothing invalidates the expressions for confidence limits given above. Confidence limits indicate the expected degree of variability in spectral estimates, any additional smoothing will reduce the variability, resulting in smaller confidence limits. Hanning can be considered as a specific case of a generalised weighting scheme which can be written as

$$\hat{f}'_{yx}(\lambda_j) = \sum_{k=-m}^{+m} w_k \hat{f}_{yx}\left(\lambda_j + \frac{2\pi k}{\mathrm{T}}\right),$$

where T is the segment length in the finite Fourier transform, and w_k; k= 0, ±1, ±2,…, ±m are the weights. It is customary for the weights to satisfy the condition: $\sum w_k = 1$. The correction to the variance of the spectral estimate is given by the factor (Brillinger, 1981)

$$\sum_{k=-m}^{+m} w_k^2 \tag{53}$$

The variance of the log transform of the auto-spectral estimate constructed from L disjoint sections with Hanning is then given by

$$\mathrm{var}\left\{\log_{10}\left(\hat{f}_{xx}(\lambda)\right)\right\} = \left(\log_{10}(\mathrm{e})\right)^2 \mathrm{L}^{-1} \sum w_k^2.$$

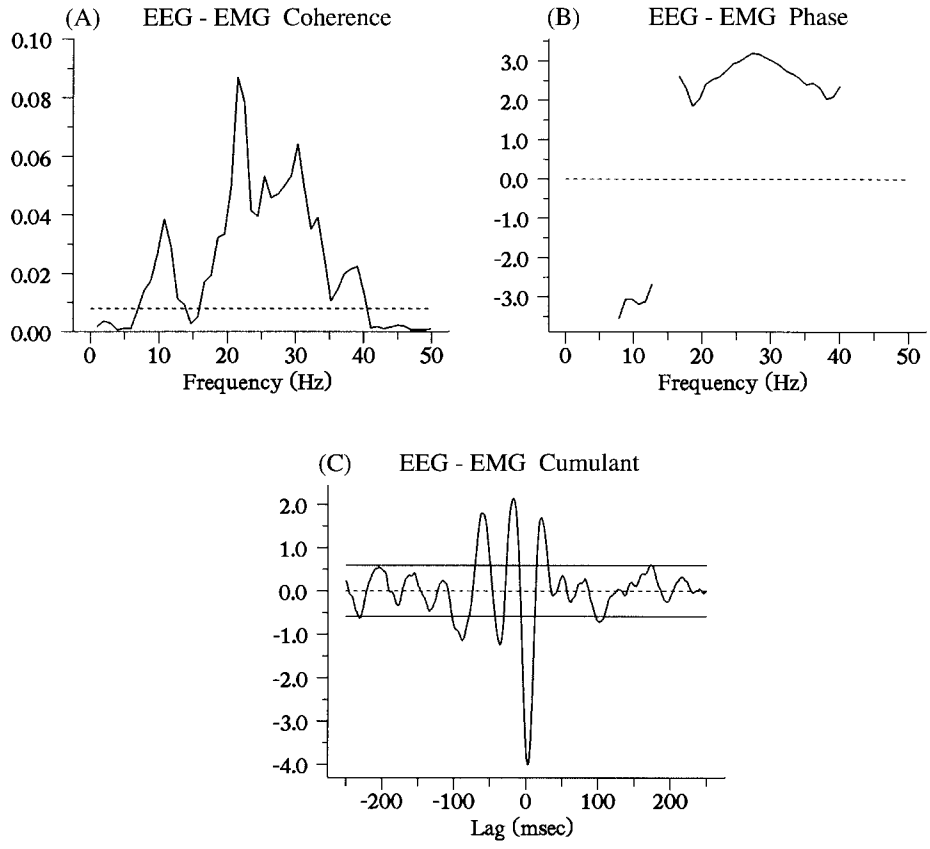

Fig. 5. Correlation between EEG and EMG during a maintained contraction. Estimate of (A) coherence, $|\hat{R}_{yx}(\lambda)|^2$, (B) phase, $\hat{\Phi}_{yx}(\lambda)$, and (C) cumulant density, $\hat{q}_{yx}(u)\times 10^4$, between a bipolar EEG recorded over the sensorimotor cortex and a surface EMG from the wrist portion of the extensor digitorum muscle. Surface EMG was full wave rectified (without time constant) before processing. Coherence and phase estimates are further smoothed with a Hanning window before plotting. The horizontal dashed line in (A) gives the estimated upper 95% confidence limit based on the assumption of independence. The phase estimate in (B) has two sections, plotted where the coherence estimate is significant, 8–12 Hz and 16–40 Hz. The horizontal lines in (C) are the asymptotic value (dashed line at zero) and estimated upper and lower 95% confidence limits, based on the assumption of independence. The EMG spectrum is illustrated in Fig. 2E, the EEG spectrum is shown in Fig. 2F.

For Hanning $\sum w_k^2 = 0.375$, which results in 95% confidence intervals for auto-spectral estimates of $\pm 0.521\, L^{-1/2}$. For coherence estimates the correction for further smoothing results in the expression

$$1-\left(0.05\right)^{1/\left((L-1)\sum w_k^2\right)} \tag{54}$$

for the upper 95% confidence limit based on the assumption of independent processes. The process of applying Hanning to spectral estimates based on (29) results in reduced variability, however, this is achieved at a cost of increased spectral bandwidth, fine structure in spectra is smoothed out by Hanning. Although the spectra are defined at the same Fourier frequencies, $\lambda_j = 2\pi j / T$, the effective spectral bandwidth of parameter estimates will be increased by the additional smoothing. In the present situation where weak correlation exists over a range of frequencies, application of Hanning results in smoother coherence and phase estimates, which better define the correlation

structure between EEG and EMG. The cumulant density is estimated from the original cross-spectral estimate, $\hat{f}_{yx}(\lambda)$, without the use of Hanning.

The coherence estimate (Fig. 5A) is significant over the range 15 to 40 Hz, with a smaller peak at 10 Hz. The maximum value of the coherence is around 0.08, which indicates weak coupling. The phase curve has two distinct sections, plotted where the coherence is significant, from 8 to 12 Hz and from 16 to 40 Hz. The cumulant has an oscillatory structure, with three clear positive peaks separate by 40 ms. This corresponds to a frequency of 25 Hz, agreeing with the coherence estimate. The cumulant has a prominent dip around time zero (minimum at +2 ms), this can be interpreted as indicating synchronous activity between the two signals. The negative value of the cumulant around time zero indicates the signals are out of phase. The phase curve (Fig. 5B) fluctuates around $\pm\pi$ radians, providing further evidence in favor of this interpretation. However, the phase section from 20 to 28 Hz has a constant slope that passes through the origin when extrapolated. A weighted regression analysis (see Appendix in Rosenberg et al., 1989) on this section gives a phase lead of 18.5±0.35 ms. In the estimate $\hat{\Phi}_{yx}(\lambda)$, the EEG, x, is the reference signal, this leads to an alternative interpretation of EMG leading EEG by around 18.5 ms over the frequency range 20–28 Hz. This latency matches the peak in the cumulant at −19 ms. This latter interpretation only explains the timing relationship between EEG and EMG over part of the frequency range at which they are correlated. A more detailed discussion of the coupling between cortical activity and motor unit firing in humans can be found in Conway et al. (1995a) and Halliday et al. (1998). This example illustrates the problems associated with interpretation of a complex correlation structure between two signals.

Example 10: EMG - EMG Correlation

The fourth example considers the interaction between two surface EMGs recorded from different muscles. The study of activation and control of co-contracting muscle groups involved in a common motor task is often referred to as the study of muscle synergy (for a review see Hepp-Raymond et al. 1996). One mechanism thought to be responsible for such muscle synergy is the presence of shared drive to the different motoneuron pools (Gibbs et al. 1995). This process can be studied experimentally by examining the cross-correlation between EMG signals recorded from the different muscles. The presence of a peak around time zero in the cross-correlation histogram is taken to reflect the presence of a common excitatory drive to both motoneuron pools (Gibbs et al. 1995). This example considers the question of muscle synergy in terms of common frequency components present in surface EMG records recorded from Abductor Digiti Minimi (ADM) and the Extensor Digitorum muscle during a postural task involving maintained wrist extension with fingers spread apart (Conway et al. 1998). The analysis of the two surface EMG signals is illustrated in Fig. 6, the data consists of four 61 second records combined to give a total of 264 seconds of data (R=264,000; T=1024; L=256). Both EMG signals were full wave rectified, without any time constant, before analysis. The log plots of the two spectral estimates, $\hat{f}_{xx}(\lambda)$ and $\hat{f}_{yy}(\lambda)$, are shown in Fig. 6A and 6B. The ADM spectrum (Fig. 6A) has a broad peak from 12 to 25Hz, the wrist extensor EMG spectrum is dominated by a sharp peak at 10 Hz. The coherence estimate (Fig. 6C) exhibits significant correlation in the range 18–26 Hz, with maximum values around 23 Hz. The phase estimate (Fig. 6D) over this frequency range exhibits a phase lead, with constant slope, for which the weighted regression scheme (Rosenberg et al., 1989) gives a time lead of 8.5±0.98 ms. The estimated cumulant (Fig. 6E) has a peak centered about −10 ms, and additional peaks around 45 ms on either side of this central peak. Both coherence and cumulant density estimates indicate a rhythmic correlation structure between the two

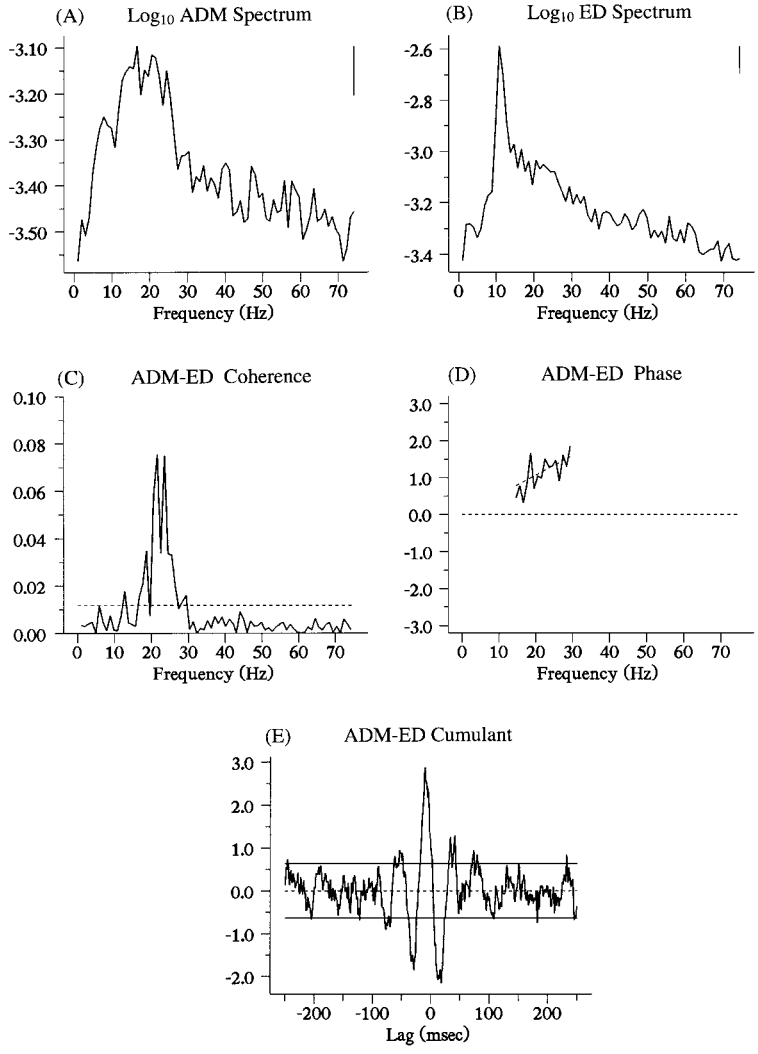

Fig. 6. Correlation between two different EMG signals during a maintained postural task. Log plot of estimated power spectra of surface EMG recorded from (A) abductor digiti minimi (ADM), and (B) wrist portion of the extensor digitorum (ED) muscle. Estimated (C) coherence, $|\hat{R}_{yx}(\lambda)|^2$, (D) phase, $\hat{\Phi}_{yx}(\lambda)$, and (E) cumulant density, $\hat{q}_{yx}(u)\times 10^4$, between the two EMG signals. Surface EMGs were full wave rectified (without time constant) before processing. Solid vertical lines at the top right in (A, B) give the estimated magnitude of a 95% confidence interval for these spectral estimates. The horizontal dashed line in (C) gives the estimated upper 95% confidence limit based on the assumption of independence. The dotted line through the phase estimate is the theoretical phase curve for a time lead of 8.5 ms. The horizontal lines in (E) are the asymptotic value (dashed line at zero) and estimated upper and lower 95% confidence limits, based on the assumption of independence.

EMG signals during the maintained contraction, suggesting that muscle synergy is in part generated by common rhythmic synaptic drive to different motor pools (Conway et al., 1998). Gibbs et al. (1995) studied correlation between EMG signals by applying a constant threshold to each EMG signal, and using a cross-correlation histogram analysis to characterize the correlation between the two sequences of spike trains generated by this thresholding of the EMG signals. This approach requires the choice of a suitable threshold. The analysis in Fig. 6 illustrates an alternative approach, which treats the rectified surface EMGs as time series.

Part 4: Multivariate Analysis

The above methods can be extended to examine the correlation structure between several simultaneously recorded signals. This is called a multivariate analysis, and is equivalent to*multivariate regression analysis*, except that parameters are estimated at each frequency of interest.

Two related questions which can be addressed by such analysis are 1) whether the correlation between two signals results from the common (linear) influence of a third signal, and 2) whether a third signal is capable of predicting the correlation between two signals. Both these questions can be addressed by estimating the *partial coherence*, *partial phase* and *partial cumulant density* which characterize the correlation between the two original signals after removing the common linear effects of the third (predictor) signal from each. This multivariate analysis can be performed on any combination of point process and/or time series data (Halliday et al., 1995a).

Partial Spectra

The starting point for the multivariate analysis are the estimates of second order spectra described in Part 2, with the requirement of three simultaneously recorded signals and spectral estimates which have been estimated with the same segment length, T. For example, to estimate the partial correlation between point process N_0 and time series x, with time series y as predictor, we start by defining partial spectra, estimates of which are then used to construct estimates of the other partial parameters. The *partial cross-spectrum* between N_0 and x, with y as predictor, is defined as (Brillinger, 1981)

$$f_{x0/y}(\lambda) = f_{x0}(\lambda) - \frac{f_{xy}(\lambda)\, f_{y0}(\lambda)}{f_{yy}(\lambda)} \tag{55}$$

The *partial auto-spectra*, $f_{xx/y}(\lambda)$, is defined as

$$f_{xx/y}(\lambda) = f_{xx}(\lambda) - \frac{f_{xy}(\lambda)\, f_{yx}(\lambda)}{f_{yy}(\lambda)} = f_{xx}(\lambda) - \frac{\left|f_{xy}(\lambda)\right|^2}{f_{yy}(\lambda)} \tag{56}$$

The other partial auto-spectrum, $f_{00/y}(\lambda)$, is defined in a similar manner. These partial spectra can be used to estimate the first order *partial coherence* between N_0 and x, with y as predictor, denoted by $\left|R_{x0/y}(\lambda)\right|^2$, as

$$\left|R_{x0/y}(\lambda)\right|^2 = \frac{\left|f_{x0/y}(\lambda)\right|^2}{f_{xx/y}(\lambda)\, f_{00/y}(\lambda)} \tag{57}$$

This equation has a similar form to that for the ordinary coherence function, (37). The corresponding first order *partial phase* is defined as

$$\Phi_{x0/y}(\lambda) = \arg\left\{f_{x0/y}(\lambda)\right\} \tag{58}$$

This function provides information about the timing relation of any residual coupling between N_0 and x after the removal of the common effects of process y. Partial coherence functions, like ordinary coherence functions, are bounded measures of association, with values between 0 and 1 (Brillinger, 1975, 1981; Rosenberg et al., 1989; Halliday et al., 1995a).

The above partial parameters can be estimated by substitution of estimates of the appropriate spectra, for example, the first order partial cross-spectrum in (55) can be estimated by:

$$\hat{f}_{x0/y}(\lambda) = \hat{f}_{x0}(\lambda) - \frac{\hat{f}_{xy}(\lambda)\,\hat{f}_{y0}(\lambda)}{\hat{f}_{yy}(\lambda)} \tag{59}$$

with the necessary second order spectra obtained from (29). The partial coherence and phase can then be estimated using direct substitution as in Part 2. The setting of confidence limits for estimates of the partial coherence (57), based on the assumption of independence, is similar to that for ordinary coherence functions, with a correction for the number of predictors used. For the case of 1 predictor, as in (57), the upper 95% confidence limit is estimated as the constant value $1-(0.05)^{1/(L-2)}$ (Halliday et al., 1995a). The setting of confidence limits about the estimated partial coherence involves the same procedures as ordinary coherence estimates, see Halliday et al. (1995a) for details.

The most convenient manner to estimate *partial cumulant density functions* is to use the inverse Fourier transform of the appropriate partial cross-spectrum. For the above three processes, this is denoted as $q_{x0/y}(u)$, which can be estimated as

$$\hat{q}_{x0/y}(u) = \frac{2\pi}{T} \sum_{|j| \le T/2b} \hat{f}_{x0/y}(\lambda_j)\, e^{i\lambda_j u} \tag{60}$$

where $\lambda_j = 2\pi j/T$ are the Fourier frequencies, and b the bin width ($b \ge 1.0$). Expression (60) is similar to (44). This function provides a measure of any residual dependency between processes N_0 and x, as a function of time, after removal of any common linear influence of process y. Expressions (45) to (47) can be used to determine a confidence limit for this estimate, under the assumptions of independence (see discussion in Halliday et al., 1995a). Equation (22) can be used for partial cumulant density estimates which involve the correlation between two point processes.

An alternative definition of the first order partial coherence, $|R_{x0/y}(\lambda)|^2$, as the magnitude squared of the correlation between the finite Fourier transforms of N_0 and x, after removal of the effects of process y from each, may be written (suppressing the dependencies on λ) as (Brillinger, 1975, 1981; Rosenberg et al., 1989; Halliday et al., 1995a)

$$|R_{x0/y}|^2 = \lim_{T\to\infty} \left| \mathrm{corr}\left\{ d_x^T - \left(\frac{f_{xy}}{f_{yy}}\right) d_y^T,\; d_{N_0}^T - \left(\frac{f_{0y}}{f_{yy}}\right) d_y^T \right\} \right|^2 \tag{61}$$

Expansion of this expression in a similar manner to (36) leads to equation (57). The two terms (f_{xy} / f_{yy}) and (f_{0y} / f_{yy}) represent the regression coefficients which give the *optimum linear prediction* of d_x^T and $d_{N_0}^T$, respectively, in terms of d_y^T. Estimates of $|R_{x0/y}(\lambda)|^2$ test the hypothesis that the coupling between N_0 and x can be predicted by process y, in which case the parameter will have the value zero.

The partial coherence defined in (57) and (61) is a first order partial coherence, which examines the correlation between two signals after removing the common effects of a single predictor. This framework can be extended to define and estimate partial coherence functions of any order. Full details, including estimation procedures and the setting of confidence limits can be found in Halliday et al. (1995a).

Results

Example 11: Partial Coherence and Cumulant

As an example of partial parameters we consider the motor unit correlation in Fig. 1, with the inclusion of the simultaneous recording of finger tremor. The hypothesis we wish to test is whether the tremor signal is a useful predictor of motor unit synchronization. This represents a multivariate analysis of the correlation between motor units N_0 and N_1 with the tremor, x, as predictor, leading to consideration of the partial coherence $|R_{10/x}(\lambda)|^2$. The spectrum of one motor unit and the tremor are shown in Fig. 2A and 2B. The correlation between the two motor units is illustrated in Fig. 3, and between one motor unit and the tremor in Fig. 4. Shown in Fig. 7 are the partial coherence estimate $|\hat{R}_{10/x}(\lambda)|^2$ and partial cumulant density estimate $\hat{q}_{10/x}(u)$. The partial coherence estimate (Fig. 7A), when compared with the ordinary coherence estimate (Fig. 3A), has almost no significant features, apart from peaks at 1 Hz and 24 Hz, indicating that the above hypothesis (that physiological tremor can predict motor unit correlation) is largely correct. The partial cumulant (Fig. 7B) has a greatly reduced central peak compared to the ordinary cumulant (Fig. 1D) and no clear sidebands. The partial phase estimate is not illustrated since it is only valid at 1 Hz and 24 Hz. This example illustrates the usefulness of a multivariate framework in testing hypotheses relating to the dependency between different signals, since we can now state conclusively that, for this data set, physiological tremor is a good predictor of motor unit synchronization.

Multiple Coherence

A second question which can be answered within a multivariate framework is the assessment of the dependence of one signal upon two or more different signals. Such a question leads to consideration of *multiple coherence functions*. For example, the multiple coherence function which assesses the strength of dependence of a time series x on

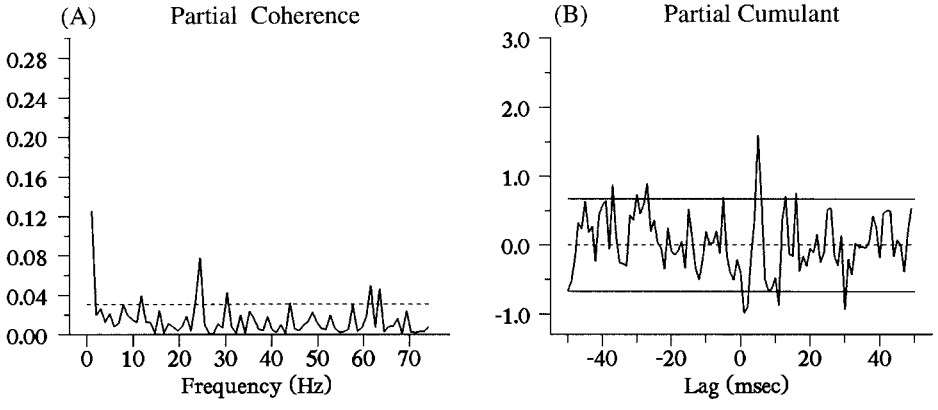

Fig. 7. Partial correlation analysis. Estimated (A) partial coherence, $|\hat{R}_{10/x}(\lambda)|^2$, and (B) partial cumulant density, $\hat{q}_{10/x}(u)\times 10^4$, between two motor units using a tremor signal as predictor. The horizontal dashed line in (A) gives the estimated upper 95% confidence limit based on the assumption of independence. The horizontal lines in (B) are the asymptotic value (dashed line at zero) and estimated upper and lower 95% confidence limits, based on the assumption of independence. The partial coherence should be compared with the ordinary coherence estimate in Fig. 3A, and the partial cumulant estimate should be compared with the ordinary cumulant estimate in Fig. 1D for the same motor unit pair.

two point processes N_0 and N_1 is denoted by $|R_{x\cdot 10}(\lambda)|^2$. This can be defined in terms of ordinary coherence and partial coherence functions between the three signals as

$$|R_{x\cdot 10}(\lambda)|^2 = |R_{x0}(\lambda)|^2 + |R_{x1/0}(\lambda)|^2 \left[1 - |R_{x0}(\lambda)|^2\right] \tag{62}$$

This function can be estimated by substituting estimates of coherence and partial coherence functions into the above equation. An example of the application of multiple coherence analysis can be found in Halliday et al. (1995a). Multiple coherence functions, like other coherence functions, are bounded measures of association with values between 0 and 1. They can also be defined for more than two predictors, the derivation and estimation procedures for such higher order multiple coherence functions is given in Halliday et al. (1995a), along with procedures for the setting of a confidence limit, based on the assumption of independence.

Comments

Multivariate parameters greatly extend the range of questions which can be addressed. In many experimental protocols designed to examine the relationship between two variables, it may not be possible (or desirable) to control other variables which influence the relationship between the two variables. In such cases, and where it is possible to record the other variables, partial parameters can be used to characterize the interdependence between all the variables, and to distinguish common effects from a direct relationship.

The derivation and estimation of partial parameters directly in the time domain depends on the types of data and requires more complex procedures. However, the Fourier based framework allows partial cumulant estimates to be constructed using identical methods to those for construction of ordinary cumulant density functions (see equations (44) and (60)). Partial cumulant density estimates can be compared with the original cumulant to provide a description of any residual coupling as a function of time.

Partial coherence estimates can only be interpreted conclusively when the partial coherence estimate exhibits a complete reduction of the coupling present in the ordinary coherence estimate (as in Fig. 7). Care should be exercised in the interpretation of a partial coherence estimate which exhibits only a part reduction in magnitude when compared with the original ordinary coherence estimate. A part reduction in magnitude can have several explanations:

- the predictor signal can only predict part of the correlation, other (unobserved) effects could exert a common influence on the two signals,
- there could be a direct causal relationship between the two signals which is independent of the effects of the predictor signal, or
- the predictor could influence the two variables in a non-linear manner (see Appendix in Rosenberg et al., 1998).

Rosenberg et al. (1989, 1998) discuss in detail the use of partial parameters to identify patterns of neuronal connectivity.

Part 5: Extended Coherence Analysis – Pooled Spectra and Pooled Coherence

The previous section dealt with a description of the correlation between many simultaneously observed signals, or dependent data. This section deals with independent data, and describes a technique which can be used to characterize a number of independent coherence estimates, the aim of which is to obtain a single measure of correlation which

is representative of the correlation between signals across a number of independent pairs of signals. The derivation below is valid for point process and/or time series data which satisfy the assumptions of weak stationarity, and the mixing condition discussed above. It is further assumed that all the original coherence estimates have been obtained from independent data sets, for example from repeat trials, or from observations across a number of subjects.

In the following definition it is assumed we are considering k independent pairs of processes, with each pair denoted by $(a_i, b_i: i=1,\ldots,k)$, and that L_i is the number of disjoint sections used to estimate the second order spectra for the i^{th} pair of processes. The processes a and b can represent any combination of point process and/or time series data. The *pooled coherence estimate* which summarizes the correlation across the k pairs of processes is obtained by a weighted average of the individual spectra as (Amjad et al., 1997)

$$\frac{\left|\sum_{i=1}^{k} \hat{f}_{a_i b_i}(\lambda)\ L_i\right|^2}{\left(\sum_{i=1}^{k} \hat{f}_{a_i a_i}(\lambda)\ L_i\right)\left(\sum_{i=1}^{k} \hat{f}_{b_i b_i}(\lambda)\ L_i\right)} \tag{63}$$

In equation (63) $\hat{f}_{a_i b_i}(\lambda)$ denotes an estimate of the second order spectrum $f_{a_i b_i}(\lambda)$, estimated from L_i disjoint sections, according to (29). The above derivation requires that all second order spectral estimates have been estimated with the same number of points in the finite Fourier transforms (24) and (26). Pooled coherence estimates, like ordinary coherence estimates, have values between 0 and 1. The upper 95% confidence limit for the estimate (63), based on the assumption of independence between the k pairs of processes, is (Amjad et al., 1997)

$$1-(0.05)^{1/(\Sigma L_i - 1)} \tag{64}$$

where ΣL_i is the total number of segments in the pooled coherence estimate. Estimated values of pooled coherence below this level at a particular frequency, λ, can be interpreted as evidence that, on average, no coupling occurs between the k pairs (a_i, b_i) at that frequency.

It is also possible to use the individual terms in expression (63) to obtain estimates of pooled spectra, which requires a correction factor of

$$\left(\sum_{i=1}^{k} L_i\right)^{-1}$$

to obtain the correct value for the two pooled auto-spectral estimates and the pooled cross-spectral estimate. Thus, the *complex valued pooled cross-spectrum* can be estimated as

$$\frac{\sum_{i=1}^{k} \hat{f}_{a_i b_i}(\lambda)\ L_i}{\left(\sum_{i=1}^{k} L_i\right)} \tag{65}$$

This can be used to obtain a *pooled phase estimate*, and a *pooled cumulant density estimate* (via an inverse Fourier transform) using methods similar to those described in Part 3. Pooled cumulant density functions provide a single time domain measure of association which can be used to summarize the correlation between many different pairs of processes. For further details see Amjad et al. (1997) and Halliday et al. (1995a).

Example 12: Pooled Coherence, Phase and Cumulant

Figure 8 illustrates an example of the application of pooled coherence to a large data set consisting of 190 individual records of motor unit pairs recorded from the third finger portion of EDC in a total of 13 healthy adult subjects during maintained postural contractions (see Conway et al., 1995b, Halliday et al., 1995a for details of experimental protocol). The average record duration is 89 seconds, range: 20 to 180 seconds. The pooled coherence, pooled phase and pooled cumulant estimates are shown in Fig. 8, constructed from a total of 16,384 segments (T=1024), equivalent to 279.6 minutes of data. Before estimating the pooled parameters, the original motor unit data underwent a temporal alignment procedure, such that the peak in individual cumulant density estimates always occurred at time zero, see Amjad et al. (1997) for further discussion of this procedure. The interpretation of these parameter estimates is similar to the ordinary coherence, phase, and cumulant density estimates shown previously, except that now we are dealing with the population behavior. The coherence estimate has two clearly defined bands, a low frequency band from 1–10 Hz, and a higher frequency band centered around 25 Hz. The magnitude of the estimate is very small, with maxima of 0.035 and

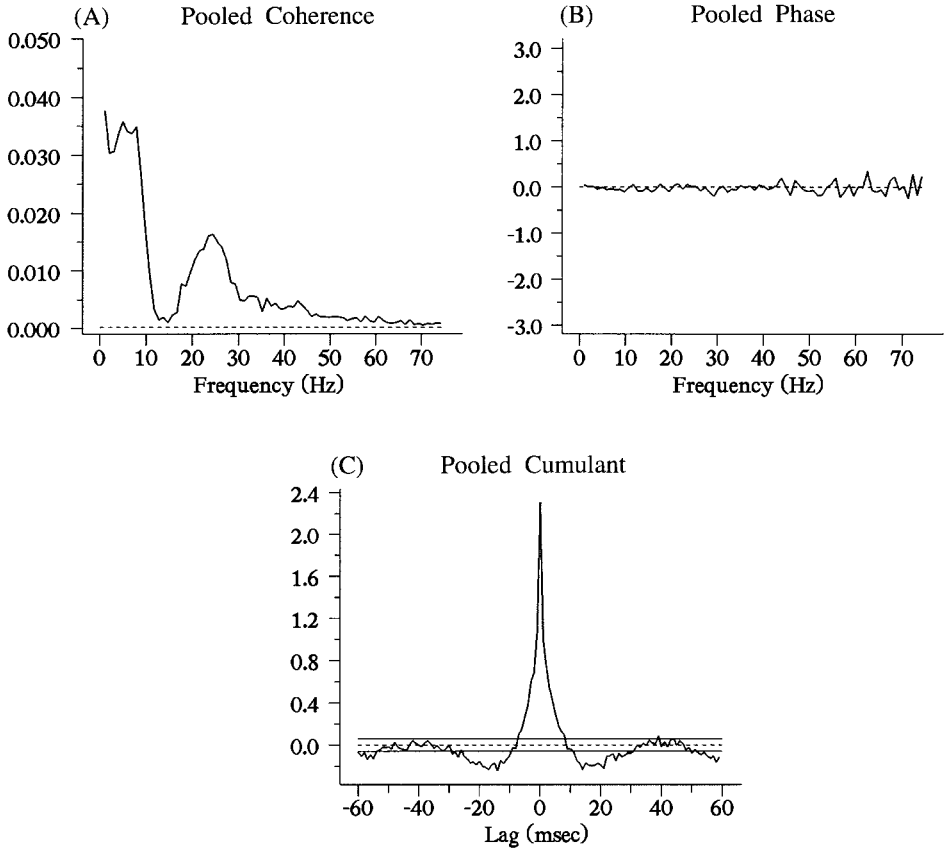

Fig. 8. Extended coherence analysis. Estimate of (A) pooled coherence, $|\hat{R}_{10}(\lambda)|^2$, (B) pooled phase, $\hat{\Phi}_{10}(\lambda)$, and (C) pooled cumulant density, $\hat{q}_{10}(u)\times 10^4$, for a population consisting of 190 separate records from motor unit pairs in EDC. The horizontal dashed line in (A) gives the estimated upper 95% confidence limit based on the assumption of independence. The horizontal lines in (C) are the asymptotic value (dashed line at zero) and estimated upper and lower 95% confidence limits, based on the assumption of independence.

0.016 in these frequency bands. The large quantity of data used to construct this estimate results in greatly reduced standard errors, which allows the weak coupling present to be more accurately specified than is possible for a single example. The estimated pooled phase is constant at zero radians, this reflects the results of the temporal alignment process. The estimated pooled cumulant has a clearly defined time course, with the central peak and sidebands well defined.

Comments

Pooled coherence analysis is useful to summarize a large data set, as in the above example. The more traditional approach is to select and present a "typical" example from the data set. However, the presentation of selected examples from a larger data set can often lead to misleading conclusions, by emphasizing features not typical of the population as a whole (see discussion in Fetz, 1992).

The framework for pooled coherence in Amjad et al. (1997) also includes a statistical test to determine if the coherence estimates in the pooled estimate can be considered to have the same magnitude at each frequency. This test provides a rigorous means of examining task-dependency in a set of coherence estimates. Amjad et al. (1997) illustrate the application of this test to investigate the relationship between a single motor unit and physiological tremor during altered inertial loading. In situations where the test for equal coherence estimates is violated, as in the above data (not shown), pooled coherence can still provide a single representative measure which summarizes the coherence structure within a larger data set.

Part 6: A Maximum Likelihood Approach to Neuronal Interactions

The Fourier based methods described in the previous sections provide a framework for analysis of spike train and/or time series data. However, they are non-parametric methods, since they do not provide estimates of parameters which have a direct neurophysiological interpretation. In this section we describe an alternative *parametric time domain* approach to analysis of neuronal interactions based on a conceptual neuron model which describes the relationship between input and output spike trains. Parameters of the model are estimated in the time domain using likelihood methods. Such an approach is commonly used in statistics to provide a model based description of data. Brillinger (1988a,b) describes a maximum likelihood approach to the analysis of neuronal interactions based on an *"integrate to threshold and fire"* model (cf. Chapter 21). This is a threshold based model which incorporates the linear summation of effects due to pre-synaptic input spikes with a recovery process, which, among other things, represents intrinsic properties of the neuron after firing an output spike. When the additive effects of the summation and recovery processes exceed threshold, the neuron will fire an action potential. An expression for the probability or likelihood of the observed output spike train is constructed in terms of a threshold-crossing probability. The arguments of this probability function depend on summation, recovery, and threshold functions. Maximum likelihood is used to estimate the parameters characterizing these functions. Breeze et al. (1994) and Emhemmed (1995) give several examples of the application of maximum likelihood to both model generated and experimental data.

The first step in the likelihood method is the construction of a *probability model for the output spike train*. We assume orderly spike train data (see Part 1), which allows spike trains to be represented as a 0–1 time series, and a standard binomial probability model to be set up for the output spike train, except that the probability of a spike oc-

curring at time t is not constant, but will depend on t. If we let N_t denote a spike train and Δ a small time interval, then at time t

$$N_t = \begin{cases} 1 & \text{if there is a spike in } (t, t+\Delta) \\ 0 & \text{otherwise} \end{cases} \tag{66}$$

for $t = 0, \pm\Delta, \pm 2\Delta, \ldots$. If H_t represents the history (or times of occurrence of spikes) of N_t up to and including t, then the conditional probability of a spike occurring at time t may be written as

$$P_t = \text{Prob}\{N_t = 1 \mid H_t\} \tag{67}$$

and the likelihood, $l(N_t, \underline{\vartheta})$, of observing a particular spike train N_t is given as (Brillinger 1988a,b; Emhemmed, 1995)

$$l(N_t, \underline{\vartheta}) = \prod_t P_t^{N_t} (1 - P_t)^{1-N_t} \tag{68}$$

where ϑ represents the set of parameters to be estimated.

Using likelihood procedures requires a model for P_t in terms of parameters that are thought to influence N_t. Following Brillinger (1988a,b) we construct a model which consists of a summation function, which describes the effects of individual input spikes, a recovery function, which accounts for refractoriness and spontaneous firing, and a random threshold function. When the combined action of the summation and recovery functions exceeds threshold, the neuron discharges an action potential and is reset to a resting level. If we denote the *summation function* as $a(u)$, the effects of an input spike train, $\underline{M(t)}$, can be modelled as a linear summation over the time of occurrence of all input spikes since the last output spike as

$$\int_0^{\gamma(t)} a(u)\, dM(t-u) = \sum_{t=0}^{\gamma_t - 1} a_u\ M_{t-u} \tag{69}$$

where $\gamma(t)$ denotes the time elapsed since the previous output spike. This equation is a linear summation of a_u over the times of occurrence of spikes, M_t, during the interval, γ_t, since the last output spike. This approach may be extended to include non-linear terms (Brillinger, 1988b), continuous (time series) inputs (Brillinger, 1988b), or a combination of time series and spike train inputs (Emhemmed, 1995).

The *recovery function* is modelled as a polynomial of the time elapsed since the last output spike, which can be written as

$$\sum_{\upsilon=1}^{k} \theta_\nu \gamma_t^\nu \tag{70}$$

where γ_t is the time since the last output spike, and θ_ν, ν=1,…k, are the parameters to be estimated. The recovery function on its own can be used to model the spontaneous discharge of a neuron.

The threshold is assumed to be either constant, θ_0, or to decay exponentially from a constant value following an output spike, which requires two extra parameters: a magnitude μ, and a time constant λ. It includes a noise term, $\varepsilon(t)$, to account for contributions from unobserved inputs which also influence the neuron. The *threshold* can be written as

$$\theta_0 + \mu e^{-\lambda t} + \varepsilon(t) \tag{71}$$

An output spike will occur when the value of the summation function and the recovery function exceed threshold.

A linear function which compares the sum of the summation and recovery functions with the threshold function, referred to as the *linear predictor*, and denoted by Z_t, can now be constructed by combining (69), (70) and (71) to give

$$Z_t = \sum_{t=0}^{\gamma_t - 1} a_u M_{t-u} + \sum_{v=1}^{k} \theta_v \gamma_t^v - (\theta_0 + \mu e^{-\lambda \gamma_t}) \tag{72}$$

A natural way to meet the requirement that the probability model for the occurrence of a spike remains between zero and one is to apply a transformation to Z_t. The function used to transform Z_t is referred to as a *link function* (McCullagh and Nelder, 1992). Brillinger (1988ab) proposes the standard cumulative normal, $\Theta(\cdot)$, as a link function, other suitable link functions are discussed in (Emhemmed, 1995). Using the standard cumulative normal the conditional probability, P_t, becomes

$$\begin{aligned} P_t &= \Theta(Z_t) \\ &= \Theta\left(\sum_{t=1}^{\gamma_t - 1} a_u M_{t-u} + \sum_{v=1}^{k} \theta_v \gamma_t^v - \left(\theta_0 + e^{-\lambda \gamma_t}\right) \right) \end{aligned} \tag{73}$$

and the corresponding likelihood function (68) is

$$l(N_t, \underline{\vartheta}) = \prod_t \Theta(Z_t)^{N_t} (1 - \Theta(Z_t))^{1 - N_t} \tag{74}$$

The set of parameters to be estimated is $\underline{\vartheta} = (\{a_u\}, \{\theta_v\}, \theta_0, \lambda, \mu)$. Maximum likelihood estimates these parameters to maximise the value of the likelihood function. This procedure may be carried out using the *statistical package GENSTAT*, which also provides standard errors for all of the estimated parameters. Emhemmed (1995) describes setting up a GENSTAT program for this analysis. An alternative implementation using the *statistical package GLIM* to investigate the relationship between three interconnected neurons is described in Brillinger (1988a).

An important aspect is assessing the *goodness of fit* of the likelihood model based on the binomial distribution. Brillinger (1988a,b) discusses a procedure for assessing the goodness of fit by comparing the estimated probability of occurrence of a spike in the modelled spike train with the theoretical probability. This procedure is based on a visual comparison between the estimated probability of occurrence of a spike in the modelled spike train with the theoretical probability when both are plotted against selected values of the linear predictor, Z_t.

Results

We illustrate the application of the likelihood method with two examples, based on analysis of data derived from a *conductance based neuron model* (Getting, 1989, Halliday, 1995), where transmembrane ionic currents are assumed to flow through channels with a linear instantaneous current voltage relationship obeying Ohm's law (Hille, 1984). The present simulations are based on point neuron models, where the intracellular membrane potential for each cell is given by the equation (Getting, 1989)

$$C_m \frac{dV_m}{dt} = -I_{leak}(V_m) - \sum_{j=1}^{n} I_{syn}^{j}(V_m, t) - \sum_{i=1}^{k} I_{ahp}^{i}(V_m, t) - I_{ext}(t) \tag{75}$$

where V_m represents the membrane potential at time t and C_m is the cell capacitance. $I_{leak}(V_m)$ is the passive leakage current, $I^{j}_{syn}(V_m,t)$ is the current due to the j^{th} pre-syn-

aptic spike, with the summation over the total number of pre-synaptic spikes, denoted by n. The afterhyperpolarization (AHP) current due to the i^{th} post-synaptic spike is $I^i_{ahp}(V_m,t)$, with the summation over the total number of post-synaptic spikes, denoted by k. $I_{ext}(t)$ is a time dependent external current applied to the cell which is used to simulate a population of unobserved inputs responsible for spontaneous background firing. In practice this is achieved by using a non-zero mean normal distribution to simulate synaptic noise (Lüscher, 1990).

The cell leakage current is estimated as $I_{leak}(V_m) = (V_m - V_r)/R_m$, where R_m is the cell input resistance. The synaptic current due to a single pre-synaptic spike at time t=0 is estimated as $I_{syn}(V_m,t) = g_{syn}(t)\,(V_m - V_{syn})$, where $g_{syn}(t)$ is a time dependent conductance change associated with the opening of ionic channels following neurotransmitter release, and V_{syn} is the equilibrium potential for this ionic current. The AHP current due to a single post-synaptic spike at time t=0 is estimated as $I_{ahp}(V_m,t) = g_{ahp}(t)\,(V_m - V_{ahp})$, where $g_{ahp}(t)$ is a time dependent conductance change, and V_{ahp} is the equilibrium potential. Expressions for $g_{syn}(t)$ and $g_{ahp}(t)$ are given below. Each pre-synaptic input spike activates one extra term in the summation over n in equation 75, which lasts for the duration of the $g_{syn}(t)$ for that input. Similarly, each post-synaptic spike activates one extra term in the summation over k in equation 75, which lasts for the duration of the $g_{ahp}(t)$ for that cell.

The voltage V_m is compared with a threshold voltage, V_{th}, at each time step to determine if an action potential has occurred. A time varying threshold is incorporated into the simulation, this allows point neuron simulations to duplicate a wide range of repetitive firing characteristics (Getting, 1989). The threshold is specified by three variables, the asymptotic level, θ_∞, the level to which the threshold is elevated after each output spike, θ_0, and the decay time constant with which the threshold decays to the asymptotic level, τ_θ.

The selection of simulation parameters is done in the same order, and at each stage parameters are selected so that the behavior of the simulation matches experimental observations for the type of cell being simulated. First passive parameters are selected, then cell membrane/input resistance, R_m, and time constant τ_m, are chosen, where $\tau_m = R_m C_m$. This determines the cell capacitance, C_m. The cell resting potential, V_r, and threshold parameters, θ_∞, θ_0 and τ_θ, are chosen. These determine the rheobase current required for repetitive firing of the cell. The time course of the AHP can be adjusted under constant current stimulus by altering the conductance function $g_{ahp}(t)$. The characteristics of a single excitatory post synaptic potential (EPSP), or a single inhibitory post synaptic potential (IPSP) from rest can be adjusted by altering the conductance $g_{syn}(t)$, and the equilibrium potential V_{syn}. The resulting EPSP or IPSP can be characterized by rise time, half width and magnitude. EPSP and IPSP conductances are modelled by an alpha function: $g_{syn}(t) = A\,(t/\tau_a)\exp(-t/\tau_a)$, (Rall, 1967) requiring the choice of a scaling factor, A, and a time constant, τ_a. Once these have been determined, the firing rates for pre-synaptic inputs have to be chosen. Selecting an appropriate mean firing rate for the input, along with any applied external current, $I_{ext}(t)$, determines the mean output firing rate of the simulation, and can be adjusted to give the desired output rate for each cell.

Example 13: Motoneuron

The first example is based on a class of cells which have been widely studied, namely motoneurons. The first simulated data set was derived from a simulation using passive parameters within the range of values quoted in Rall (1977) for experimental studies on spinal motoneurons, with R_m=5 MΩ, τ_m=5ms, C_m= 1μF, and a resting potential of V_r=

–70 mV. The AHP conductance used a simplified version of the three-term model proposed by Baldissera and Gustafsson (1974) for observed AHP time courses in cat lumbar motoneurons, based on an exponential conductance function $g_{ahp}(t) = A \exp(-t/\tau_a)$, with τ_a=14 ms, and A=1.0e–08, with V_{ahp}=–75 mV. The threshold parameters were θ_∞= –65 mV, θ_0=–55 mV, and τ_θ=20 ms. In this example, no synaptic noise was applied, the output discharge was entirely due to the single pre-synaptic input, which was activated by a random, or Poisson, spike train with a mean firing rate of 50 spikes/s. The EPSP conductance values were τ_a=2 ms, and A=1.1e^{-08}, with V_{syn}=0.0 mV. The EPSP parameters for a single conductance activated from rest are a rise time (10%–90%) of T_r=3.1 ms, a half width of T_{hw}=9.8 ms, and a magnitude of 10.62 mV. These values are outside the upper limits of 2.1 ms, 7.7 ms and 0.54 mV reported for the same parameters measured using spike triggered averaging of single fibre Ia connections to cat spinal motoneurons (Cope et al., 1987), but were necessary, however, to obtain repetitive firing with only a single pre-synaptic input. The EPSP magnitude and duration during repetitive firing are reduced due to the shunting action of the large AHP conductance. The simulation was used to generate 60 seconds of data at 1 ms sampling intervals with these parameters, in total 2416 output spikes were obtained, a mean rate of 40.3 spikes/s.

Illustrated in Fig. 9A is the estimated cumulant density, $\hat{q}_{10}(u)$, see equation (16), between the input and output spike trains. This estimate suggests individual inputs have an excitatory effect on the output discharge, the duration of which is about 4 ms. There is a subsequent dip in the estimated cumulant which is outside the lower 95% confidence limit, however, this feature can be interpreted to reflect the mapping to the cumulant density of structure in the auto-correlation of the output discharge (Moore et al., 1970). In contrast, the likelihood approach separates out these two effects. The estimated summation function, Fig. 9C, which we denote by $\hat{a}(u)$, has significant values for lags up to 7 ms, suggesting that the duration of the excitatory effect for a single input lasts about 7 ms. The recovery function used a third order polynomial, k=3 in equation (70), however, using a threshold with an exponential term results in values of θ_2 and θ_3 which were not significant, and can be neglected, resulting in a first order recovery function with constant slope. The difference between the estimated recovery and threshold functions (Fig. 9E) indicates that the probability of an output spike is small up to about 15 ms after an output spike, after which they converge more rapidly, indicating an increase in firing probability. The features of the summation, recovery, and threshold function correspond well with the structure of the simulated motoneuron, in which the half width of a single excitatory postsynaptic potential was 9.8 ms, and the mean rate of the output spike train was 40 spikes/s.

Example 14: Invertebrate Neuron

In the second example the simulated neuron is based on studies of small networks responsible for rhythmic pattern generation in invertebrates (Getting, 1989). The simulation was set up with parameters R_m=12.5 MΩ, τ_m=50 ms, giving C_m=4 μF, and a resting potential of V_r=–60 mV. The threshold parameters were θ_∞=–45 mV, θ_0=–35 mV, and τ_θ=10 ms. Synaptic noise was simulated by an applied $I_{ext}(t)$ with a mean value of 2.9 nA, and a standard deviation of 1.7 nA. In this example an inhibitory input was applied, with conductance parameters of τ_a=1 ms, A=2.2e^{-07}, and V_{syn}=–80.0 mV. The IPSP parameters for a single conductance activated from rest were T_r=5.7 ms, T_{hw}=39.9 ms, and a magnitude of –1.0 mV. The input firing rate was set at 50 spikes/s with a random discharge, and in 60 seconds the simulation produced 1400 output spikes, 23.3 spikes/s. The estimated cumulant density, Fig. 9B, suggests an inhibitory effect lasting about 8 ms fol-

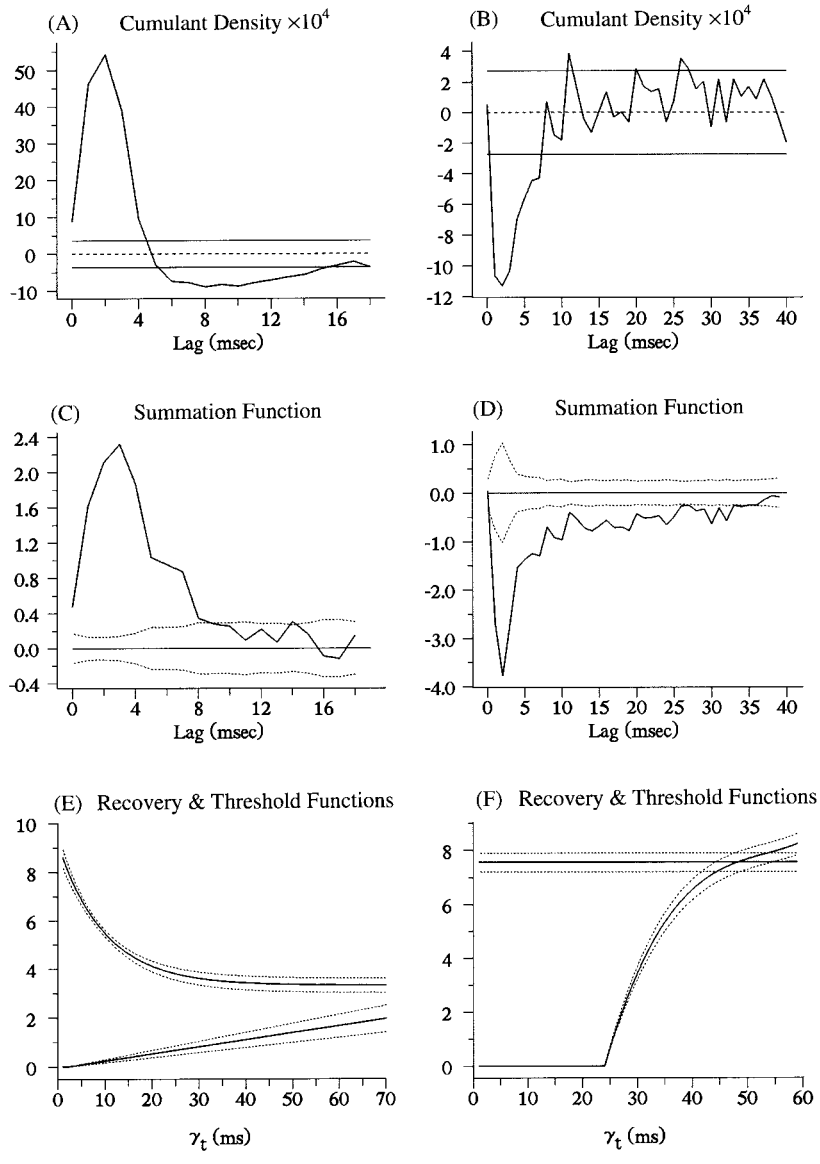

Fig. 9. (A) Estimated cumulant density, $\hat{q}_{10}(u)\times10^4$, between a random excitatory spike train input and the output discharge for a simulated neurone. (C) Estimated summation function, $\hat{a}(u)$, and (E) estimated threshold function (upper traces) and recovery function (lower traces) for the same data set as in (A). (B) Estimated cumulant density, $\hat{q}_{10}(u)\times10^4$, between a random inhibitory spike train input and the output discharge for a simulated neurone. (D) Estimated summation function, $\hat{a}(u)$, and (F) estimated threshold function (upper traces) and recovery function (lower traces) for the same data set as in (B). Horizontal lines in (A, B) indicate the asymptotic value (dashed line at zero) and estimated upper and lower 95% confidence limits, based on the assumption of independence. Dotted lines in (C, D) indicate ±1.96 standard error limits plotted around zero. Dotted lines in (E, F) represent ±1.96 standard error limits for threshold and recovery function estimates.

lowing each input spike, whereas the summation function (Fig. 9D) suggests that the inhibitory effect lasts for more than 30 ms, which corresponds more closely with the 40 ms half width of a single inhibitory post synaptic potential. This example uses a constant threshold in the likelihood model, the recovery function is fixed at zero for lags up to

25 ms, which is the minimum interspike interval for the output discharge, after this the recovery function, modelled by a third order polynomial, rises quickly, indicating a rapid increase in the probability of firing. In the output discharge there are only 43 intervals which exceed 60 ms.

Comments

These two examples illustrate the application of likelihood methods to describe the input/output relationship for neuronal data. The estimated parameters have a direct neurophysiological interpretation, the summation function matches closely the time course of individual EPSP and IPSP functions. The estimated recovery and threshold functions give insight into intrinsic properties and refractory behavior after firing. This is in contrast to the non-parametric cross-correlation based estimates where effects due to single inputs and intrinsic effects contribute to the time course of the estimated cumulant density. It is worth pointing out that in both these examples random (Poisson) input sequences were used in an attempt to minimise this effect.

The likelihood analysis is based on an "integrate to threshold and fire" model which incorporates a random threshold, and where output spike times are determined by a threshold-crossing process. An important assumption in likelihood analysis is that the underlying model is valid. In this context, the biophysically motivated conductance based model (Getting, 1989) used to generate the data for the two examples is similar in form to the conceptual likelihood model. This suggests that the likelihood model will be useful to investigate a variety of neuronal spike train data. Examples of the application to experimental data are given in Brillinger (1988a,b) and Emhemmed (1995). The likelihood method is flexible, and allows for arbitrary numbers of neurons and neuronal mechanisms, which can be incorporated by the addition of extra terms in the linear predictor, equation (72).

Likelihood analysis is computationally more intensive that the Fourier based methods presented above. However, if the aim of an analysis is to obtain estimates of parameters of models which underlie neuronal processes, the likelihood approach may be more appropriate. An initial analysis using Fourier based techniques can provide guidance in the types of model which should be considered.

Concluding Remarks

In this chapter we have presented a framework for the analysis of neurophysiological data, which includes both time and frequency domain parameters. The framework relies on Fourier based estimation methods, which provides a unified framework for the analysis of both data types encountered in neuroscience (spike train and/or waveform data). Time domain parameters are closely related to the more traditionally used cross-correlation histogram and spike triggered averaging methodologies. Two extensions of the Fourier based framework have also been described, which extend the range of questions which can be addressed. A multivariate framework which can deal with the relationship between several simultaneously recorded signals was described in Part 4. The extended coherence analysis described in Part 5 can be used to summarize the correlation structure within a large number of data sets, and to explore questions of task dependency. Both these extensions use Fourier estimation methods, however, equivalent time domain parameters can be obtained by an inverse Fourier transform. In Part 3 we stress the complementary nature of time and frequency domain parameters for characterizing the correlation structure between neural signals. Part 6 outlines an alternative parametric time domain model based approach to characterizing neuronal spike train data.

Throughout the chapter we have stressed the importance of using confidence limits on parameter estimates. In most cases the expressions are easy to compute. The use of confidence limits are an essential part of any statistical analysis, both for dealing with uncertainty in parameter estimates, and for testing hypothesis. Their use is illustrated in the examples presented in this chapter, for example in distinguishing between distinct rhythmic components and chance fluctuations in spectral estimates (see Fig.2), and in testing the hypothesis that the estimated correlation between two signals exceeds that expected by chance (Figs. 1, 3, 4, 5, 6, 8). The duration of the individual data sets in these examples ranges from 89,000 points to 264,000 points. The inferences which can be made from analysis of these data are a result, in part, of the large numbers of points in these data sets. Analysis of data sets which consist of a few thousand points, or less, without the use of confidence limits may lead to misinterpretation of parameter estimates, particularly in situations involving weak correlation, since the uncertainty in parameter estimates may have a similar order of magnitude as the parameter being estimated. In addition, over-interpretation of apparent fine details in parameter estimates may also give misleading results without careful use of confidence limits for parameter estimates. The setting of confidence limits about estimated values of coherence is described in Halliday et al. (1995a, Section VI). For time domain parameter estimates the sampling distribution for parameter estimates is more complex, and are only valid under the restricted condition of independent processes (see Amjad et al. 1997). In applying these techniques, it is important to distinguish between a parameter and its estimate, all parameter estimates have error and uncertainty, partly due to the problem of estimation associated with finite quantities of data. The use of raw cross-correlation histograms and raw spike triggered averages should therefore be avoided if possible. It seems appropriate to quote from one of the first studies to apply the cross-correlation technique to spike train data (Griffith and Horn, 1963): "… it is essential to have some idea of what deviations may be regarded as significant …".

The above comments are not intended to discourage the potential user. Interpretation of parameter estimates cannot be done according to a set of pre-defined rules. Confidence limits only provide a guide to interpretation, the user should also be guided by their knowledge of the system under study. Nonetheless, these techniques do provide a comprehensive framework for analysis of neurophysiological data (and other types of signals which meet the assumptions of weak stationarity, mixing condition, and orderliness for point process data). The multivariate methods in Part 4 are particularly suited to take advantage of experimental developments involving multi-electrode recording techniques (cf. Chapter 17). Correlation analysis has underpinned many developments in neuroscience, and can continue to contribute to many studies which address questions related to tracing signal pathways, to the relationship between cortical activity, electromyographic activity and motor output, to studying the relationship between distant neural groups, and to issues related to information processing in neural circuits, and other dynamic aspects of neural behavior. The experimental data presented in this chapter are all from normal subjects, we conclude by commenting that these methods are equally applicable to clinical studies.

Analysis Software

A software archive is available to perform some of the above analyses. Details of this archive can be obtained by sending an e-mail request to: gpaa34@udcf.gla.ac.uk.

Acknowledgement: Supported by grants from The Wellcome Trust (036928; 048128), and the Joint Research Council/HCI Cognitive Science Initiative. We would like to thank Peter Breeze and Yousef Emhemmed for their help in preparing the section on maximum likelihood.

References

Amjad AM, Halliday DM, Rosenberg JR, Conway BA (1997) An extended difference of coherence test for comparing and combining independent estimates: theory and application to the study of motor units and physiological tremor. J. Neurosci. Meth. 73: 69–79

Baldissera F, Gustafsson B (1974) Afterhyperpolarization conductance time course in lumbar motoneurones of the cat. Acta Physiol Scand 91: 512–527

Bartlett MS (1948) Smoothing periodograms from time series with continuous spectra. Nature 161: 686–687

Bartlett MS (1963) The spectral analysis of point processes. J Roy Statist Soc 25: 264–281

Blackman RB, Tukey JW (1958) The measurement of power spectra from the point of view of communications engineering. Bell Sys Tech J 37: 183–282, 485–569 (Reprinted Dover Press, New-York, 1959)

Bloomfield P(1976) Fourier Analysis of Time Series: An Introduction. Wiley, New York.

Breeze P, Emhemmed YM, Halliday DM, Rosenberg JR (1994) Likelihood analysis of a model for neuronal input-output data. J Physiol 479P: 112P

Brillinger DR (1972) The spectral analysis of stationary interval functions. In: LeCam LM, Neyman J, Scott E (eds) Proceedings 6th Berkeley Symposium Mathematics Statistics Probability, Univ California Press, Berkeley, pp 483–513

Brillinger DR (1974) Fourier analysis of stationary processes. Proc IEEE 62: 1628–1643

Brillinger DR (1975) Identification of point process systems. Ann Probability 3: 909–929

Brillinger DR (1976) Estimation of second-order intensities of a bivariate stationary point process. J Roy Statist Soc B38: 60–66

Brillinger DR (1978) Comparative aspects of the study of ordinary time series and of point processes. In: Krishnaiah PR (ed) Developments in Statistics, vol 1. Academic Press, New York, pp 33–133

Brillinger DR (1981) Time Series – Data Analysis and Theory, 2nd edn. Holden Day, San Francisco

Brillinger DR (1983) The finite Fourier transform of a stationary process. In: Brillinger DR, Krishnaiah PR (eds) Handbook of Statistics, Elsevier, pp 21–37

Brillinger DR (1988a) Maximum likelihood analysis of spike trains of interacting nerve cells. Biol Cybernet 59: 198–200

Brillinger DR (1988b). The maximum likelihood approach to the identification of neuronal interactions. Ann Biomed Eng 16: 3–16

Brillinger DR, Tukey JW (1984) Spectrum analysis in the presence of noise: Some issues and examples. In: The collected works of John W Tukey, Volume II, Time series: 1965–1984. Wadsworth , Belmont, CA, pp 1001–1141

Conway BA, Halliday DM, Rosenberg JR (1993) Detection of weak synaptic interactions between single Ia-afferents and motor-unit spike trains in the decerebrate cat. J Physiol 471: 379–409

Conway BA, Halliday DM, Farmer, SF, Shahani U, Maas P, Weir AI, Rosenberg JR (1995a) Synchronization between motor cortex and spinal motoneuronal pool during the performance of a maintained motor task in man. J Physiol 489: 917–924

Conway BA, Farmer, SF, Halliday DM, Rosenberg JR (1995b) On the relation between motor unit discharge and physiological tremor. In: Taylor A, Gladden MH, Durbaba R (eds) Alpha and Gamma Motor Systems. Plenum Press, New York, pp 596–598

Conway BA, Halliday DM, Bray K, Cameron M, McLelland D, Mulcahy E, Farmer SF, Rosenberg JR (1998) Inter-muscle coherence during co-contraction of finger and wrist muscles in man. J Physiol 509: 175P

Cope TC, Fetz EE, Matsumura M (1987) Cross-correlation assessment of synaptic strength of single Ia fibre connections with triceps surae motoneurones in cats. J Physiol 390: 161–188

Cox DR (1965) On the estimation of the intensity function of a stationary point process. J Roy Statist Soc B27: 332–337

Cox DR, Isham V (1980) Point Processes. Chapman and Hall, London

Cox DR, Lewis PAW (1972) Multivariate point processes. In: LeCam LM, Neyman J, Scott E (eds) Proceedings 6th Berkeley Symposium Mathematics Statistics Probability, vol 3. University of California Press, Berkeley pp 401–488

Daley DJ, Vere-Jones D (1988) An introduction to the Theory of Point Processes. Springer, New York

Datta AK, Stephens JA (1990) Short-term synchronization of motor unit activity during voluntary contractions in man. J Physiol 422: 397–419

Emhemmed YM (1995) Maximum likelihood analysis of neuronal spike trains. PhD Thesis, University of Glasgow, 246pp

Fetz EE (1992) Are movement parameters recognizably coded in the activity of single neurons. Behavioral Brain Sci, 15: 679–690
Farmer SF, Bremner FD, Halliday DM, Rosenberg JR, Stephens JA (1993) The frequency content of common synaptic inputs to motoneurones studied during voluntary isometric contraction in man. J Physiol 470: 127–155
Getting PA (1989) Reconstruction of small networks. In: Koch C, Segev I (eds) Methods in neuronal modeling: From synapses to networks, MIT Press, pp 171–194
Gibbs J, Harrison LM, Stephens JA (1995) Organization of inputs to motoneuron pools in man. J Physiol, 485: 245–256
Griffith JS, Horn G (1963) Functional coupling between cells in the visual cortex of the unrestrained cat. Nature, 199: 873, 893–895
Halliday DM, Murray-Smith DJ, Rosenberg JR (1992) A frequency domain identification approach to the study of neuromuscular systems – a combined experimental and modelling study. Trans Inst MC, 14: 79–90
Halliday DM (1995) Effects of electronic spread of EPSPs on synaptic transmission in motoneurones – A simulation Study. In: Taylor A, Gladden MH, Durbaba R (eds) Alpha and Gamma Motor Systems. Plenum Press, New York, pp 337–339
Halliday DM, Rosenberg JR, Amjad AM, Breeze P, Conway BA, Farmer SF (1995a) A framework for the analysis of mixed time series/point process data – Theory and application to the study of physiological tremor, single motor unit discharges and electromyograms. Prog Biophys molec Biol, 64: 237–278
Halliday DM, Kakuda N, Wessberg J, Vallbo ÅB, Conway BA, Rosenberg JR (1995b) Correlation between Ia afferent discharges, EMG and torque during steady isometric contractions of human finger muscles. In: Taylor A, Gladden MH, Durbaba R (eds) Alpha and Gamma Motor Systems. Plenum Press, New York, pp 547–549
Halliday DM, Conway BA, Farmer SF, Rosenberg JR (1998) Using electroencephalography to study functional coupling between cortical activity and electromyograms during voluntary contractions in humans. Neurosci Lett, 241: 5–8
Hille B (1984) Ionic channels of excitable membranes. Sinauer
Henneman E, Mendell LM (1981) Functional organization of motoneuron pool and its inputs. In: Brookhart JM, Mountcastle VB (eds) Handbook of Physiology, Section 1, Vol 2, Part 1, The nervous system: Motor control. American Physiological Society, Bethesda, MD, pp 423–507
Hepp-Raymond M-C, Huesler EJ, Maier MA (1996) Precision grip in humans: Temporal and spatial synergies. In: Wing AM, Haggard P, Flanagan JR (eds) Hand and Brain, the neurophysiology and psychology of hand movements. Academic Press, London, pp 37–68
Jenkins GM, Watts DG (1968) Spectral analysis and its applications. Holden-Day.
Kendall DG, Stuart A (1966) The advanced theory of statistics, vol 1. Griffin, London. Kirkwood PA, Sears TA (1978) The synaptic connections to intercostal motoneurones revealed by the average common excitation potential. J Physiol, 275: 103–134
Kirkwood PA, Sears, TA (1980) The measurement of synaptic connections in the mammalian central nervous system by means of spike triggered averaging. In: Desmedt JE (ed) Progress in Clinical Neurophysiology, vol 8, Spinal and supraspinal mechanisms of voluntary motor control and locomotion. Basel, S Karger, pp 44–71
Lüscher H-R (1990) Transmission failure and its relief in the spinal monosynaptic reflex arc. In: Binder MD, Mendell LM (eds) The segmental motor system, Oxford University Press, pp 328–348 McCullagh P, Nelder JA (1992) General Linear Models (2nd edition). Monographs on statistics and Applied Probability 37. Chapman Hall, London
Mendel J (1991) Tutorial on higher-order statistics (spectra) in signal processing and system theory: theoretical results and some applications. Proc IEEE, 79: 278–305
Mendell LM, Henneman E (1968) Terminals of single Ia fibres: Distribution within a pool of 300 homonymous motoneurones. Science 160: 96–98
Mendell LM, Henneman E (1971) Terminals of single Ia fibres: location, density and distribution within a pool of 300 homonymous motor neurons. J Neurophysiol, 34: 171–187
Moore GP, Segundo JP, Perkel DH, Levitan H (1970) Statistical signs of synaptic interaction in neurones. Biophys J 10: 876–900
Parzen E (1961) Mathematical considerations in the estimation of spectra. Technometrics, 3: 167–190 Press WH, Flannery BP, Teukolsky SA, Vetterling WT (1989) Numerical recipes. Cambridge University Press
Rall W (1967) Distinguishing theoretical synaptic potentials computed for different soma-dendritic distributions of synaptic inputs. J Neurophysiol 30: 1138–1168

Rall W (1977) Core conductor theory and cable properties of neurones. In: Kandel ER, Brookhart JM, Mountcastle VB (eds) Handbook of physiology: The nervous system, vol 1, part 1. Williams and Wilkins, Maryland, pp 39–97

Rigas A (1983) Point Processes and Time Series Analysis: Theory and Applications to Complex Physiological Systems. PhD Thesis, University of Glasgow, 330pp

Rosenberg JR, Murray-Smith DJ, Rigas A (1982) An introduction to the application of system identification techniques to elements of the neuromuscular system. Trans Inst MC 4: 187–201

Rosenberg JR, Amjad AM, Breeze P, Brillinger DR, Halliday DM (1989) The Fourier approach to the identification of functional coupling between neuronal spike trains. Prog Biophys molec Biol, 53: 1–31

Rosenberg JR, Halliday DM, Breeze P, Conway BA (1998) Identification of patterns of neuronal activity – partial spectra, partial coherence, and neuronal interactions. J Neurosci Meth 83:57–72

Rosenblatt M (1983) Cumulants and Cumulant Spectra. In: Brillinger DR, Krishnaiah PR (eds) Handbook of Statistics vol 3. North Holland, New York, pp 369–382

Schuster A (1898) On the investigation of hidden periodicities with application to a supposed 26 day period of meteorological phenomenon. Terr Mag, 3: 13–41

Sears TA, Stagg D (1976) Short-term synchronization of intercostal motoneurone activity. J Physiol 263: 357–387

Sorensen HV, Jones DL, Heideman MT, Burrus CS (1987) Real valued Fast Fourier Transform Algorithms. Proc IEEE ASSP, 35: 849–863; Corrections p 1353

Srinivasan SK (1974) Stochastic Point Processes and their Applications. Monograph No 34. Griffin, London

Stauffer EK, Watt DGD, Taylor A, Reinking RM, Stuart DG (1976) Analysis of muscle receptor connections by spike triggered averaging. 2. Spindle group II afferents. J Neurophysiol, 39: 1393–1402

Stiles RN, Randall JE (1967) Mechanical factors in human tremor frequency. J App Physiol 23: 324–330

Tukey JW (1961) Discussion, emphasizing the connection between analysis of variance and spectrum analysis. Technometrics, 3: 191–219

Tukey JW (1980) Can we predict where "time series" should go next? In: Brillinger DR, Tiao GC(eds) Directions in Time Series IMS, Hayward, California, pp 1–31

Vallbo ÅB, Hagbarth K-E (1968) Activity from skin mechanoreceptors recorded percutaneously in awake human subjects. Exp Neurol 21: 270–289

Watt DGD, Stauffer EK, Taylor A, Reinking RM, Stuart DG (1976) Analysis of muscle receptor connections by spike triggered averaging. I. Spindle primary and tendon organ afferents. J Neurophysiol 39: 1375–1392

Wiener N (1930) Generalized harmonic analysis. Acta Math 55: 117–258